


RESEARCH ARTICLE

Cite this: *RSC Med. Chem.*, 2022, **13**, 1082

Synthesis and *in vitro* anticancer evaluation of novel flavonoid-based amide derivatives as regulators of the PI3K/AKT signal pathway for TNBC treatment†

Dailong Zha,‡ Yuanzhi Li,‡ Yingqi Luo,‡ Yingfan Liu,‡ Zehong Lin, Chujie Lin, Siyue Chen, Jiangping Wu, Lihong Yu, Shaobin Chen, Peiquan Zhang, Wenhao Wu* and Chao Zhang *

Aberrant activation of the PI3K/AKT pathway is considered in many malignant tumors and plays a crucial role in mediating malignancy progression, metastasis, and chemoresistance. Consequently, development of PI3K/AKT pathway targeted drugs is currently an attractive research field for tumor treatment. In this study, twenty-six flavonoid-based amide derivatives were synthesized and evaluated for their antiproliferation effects against seven cancer cell lines, including MDA-MB-231, MCF-7, HCC1937, A549, HepG2, GTL-16 and HeLa. Among them, compound **7t** possessed the best specific cytotoxicity against triple negative breast cancer MDA-MB-231 cells with an IC_{50} value of $1.76 \pm 0.91 \mu\text{M}$ and also presented inhibitory ability on clonal-formation, migration and invasion of MDA-MB-231 cells. Further cell-based mechanistic studies demonstrated that compound **7t** caused cell cycle arrest of MDA-MB-231 cells at the G_0/G_1 phase and induced apoptosis. Meanwhile, the western blot assay revealed that compound **7t** could down-regulate the expression of p-PI3K, p-AKT, and Bcl-2 and up-regulate the production of PTEN, Bax, and caspase-3. Molecular docking also showed a possible binding mode of **7t** with PI3K α . Together, compound **7t** was eligible as a potential TNBC therapeutic candidate for further development.

Received 17th May 2022,
Accepted 18th July 2022

DOI: 10.1039/d2md00148a

rsc.li/medchem

1. Introduction

Despite efforts over the last 20 years to find effective therapeutic medicines, cancer remains a global concern. According to the statistics of the World Health Organization in 2020,¹ cancer was the top cause of death in 185 nations globally and more than 2.26 million cases were newly recorded. Among them, breast cancer has taken over lung cancer as the leading cause of female death. Despite the fact that conventional medications, combination therapies, and targeted treatments have significantly improved 5 year survival rates, patients with high-grade and metastatic malignancies still encounter a poor outlook.² The molecular etiology of most cancers has not been completely elucidated

and some types of cancer still lack efficient therapeutic drugs, resulting in a huge challenging and urgent demand to develop highly effective therapies.

Phosphatidylinositol 3-kinases (PI3Ks) are a family of lipid kinases associated with oncogene products which are one of the significant upstream components of the PI3K/AKT signal transduction pathway that has tremendous impact on tumor occurrence and development,³ whereas AKT is a downstream component of this pathway.^{4,5} In response to stimulation by growth factors such as VEGF, HGF, insulin or signal transduction complexes, RTKs and GPCRs on the cell membrane are activated, promoting the phosphorylation response of PI3K and leading to the initiation of the PI3K/AKT pathway.^{6,7} Generally, the activated PI3K catalyzes the phosphorylation of phosphatidylinositol-4,5-bisphosphate (PIP2) to phosphatidylinositol-3,4,5-trisphosphate (PIP3) with second messenger function.⁸⁻¹⁰ PIP3 then binds to the N-terminal PH domain of AKT and aggregates it to the plasma membrane, where AKT is activated by phosphorylating the Thr308 and Ser473 residues of PDK1 and PDK2, respectively.¹¹ The activated AKT is subsequently detached from the cell membrane and released into the nucleus or free in the cytoplasm to further activate related

Guangzhou Municipal and Guangdong Provincial Key Laboratory of Molecular Target & Clinical Pharmacology, The NMPA and State Key Laboratory of Respiratory Disease, School of Pharmaceutical Sciences and the Fifth Affiliated Hospital, Guangzhou Medical University, Guangzhou 511436, China.

E-mail: wenhao_wu@gzhmu.edu.cn, chao-zh@163.com

† Electronic supplementary information (ESI) available. See DOI: <https://doi.org/10.1039/d2md00148a>

‡ These authors contributed equally to this work.

downstream proteins that regulate cell growth, apoptosis, invasion, metastasis, and angiogenesis.^{12,13} Consequently, the PI3K/AKT pathway plays a crucial role in regulation of multiple physiological processes critical to mediate malignancy progression, metastasis, and chemoresistance.^{14–16} Hyper-activation of such a pathway is considered a common event in cancers including breast, non-small cell lung, and colorectal cancers.^{17–19} As multiple pathways contribute to the activation of the PI3K/AKT pathway, investigation of drugs targeting this system can provide new options for potent tumor therapies.²⁰

As mentioned previously, development of a PI3K/AKT pathway targeted regulatory agent is currently an attractive research field in view of the significance for tumor treatment.^{21–23} Some typical PI3K/AKT inhibitors are depicted in Fig. 1. Galangin is a natural flavonoid with strong antiproliferation and apoptosis induction activities against many cancer cells, such as breast, melanoma, lung, and liver cancers through targeting the PI3K/AKT signal pathway.^{24–27} Wortmannin is an irreversible PI3K inhibitor isolated from fungal metabolites, which possesses obvious cytotoxicity and kinase inhibitory potency.²⁸ However, its low bioavailability and high toxicity limit its clinical value. LY294002 is a reversible PI3K inhibitor originating from the natural flavonoid quercetin,²⁹ which can decrease the formation of tumor tissue and autophagosomes by influencing the cell cycle and inducing cell apoptosis.³⁰ But the clinical application is restricted due to its short half-life, poor lipid solubility, low bioavailability, and susceptibility to metabolic inactivation.^{31–33} BKM120 (Buparlisib) is a broad-spectrum PI3K inhibitor with high oral bioavailability, which can not only suppress the expression of NRF2 and enhance the sensitivity of Keap1 or NFE2L2 mutant squamous cell lung cancer, but also block VEGF induced neovascularization.^{34,35} Unfortunately, the phase III clinical research of BKM120 has

been terminated because of its toxicity. Thus, exploration of low toxicity PI3K/AKT pathway inhibitors remains challenging.

Our group make continuous efforts to explore new anticancer candidates³⁶ and have developed a kind of ligustrazine–chalcone hybrid as an anti-triple negative breast cancer (TNBC) agent in the previous study.³⁷ Thus, inspired by the efficacy of flavonoids having an outstanding anticancer activity *via* targeting the PI3K/AKT pathway^{38,39} and structural relevance between flavonoids and chalcone, we herein report the synthesis of flavonoid-based amide derivatives and evaluation of their anticancer ability. Analysis of the structural characteristics of the target compounds shows that a 4-fluorophenyl and diverse amides were introduced at the 7- and 3'-positions of the benzopyran-4-one mother nucleus respectively. Compared to galangin and LY294002, removal of excess hydroxyl groups at 5- and 7-positions could avoid inactivation of glycosylation metabolism, and introduction of the amide group and fluorine atom was expected to improve the anticancer capability. The anticancer evaluation involved cytological experiments and Western blot assay. The former was performed to assess the *in vitro* antiproliferative effect and related mechanism, while the latter was used to determine the influence of potential compounds on the expression of PI3K/AKT signal pathway related proteins.

2. Results and discussion

2.1 Chemistry

The synthetic routine of target compounds 7a–7z is described in Scheme 1. Initially, the Suzuki–Miyaura coupling reaction was conducted between 1-(4'-bromo-2-hydroxyphenyl) ethan-1-one 1 and (4-fluorophenyl) boronic acid 2 to give intermediate 3. It was then reacted with 3-aminobenzaldehyde *via* aldol

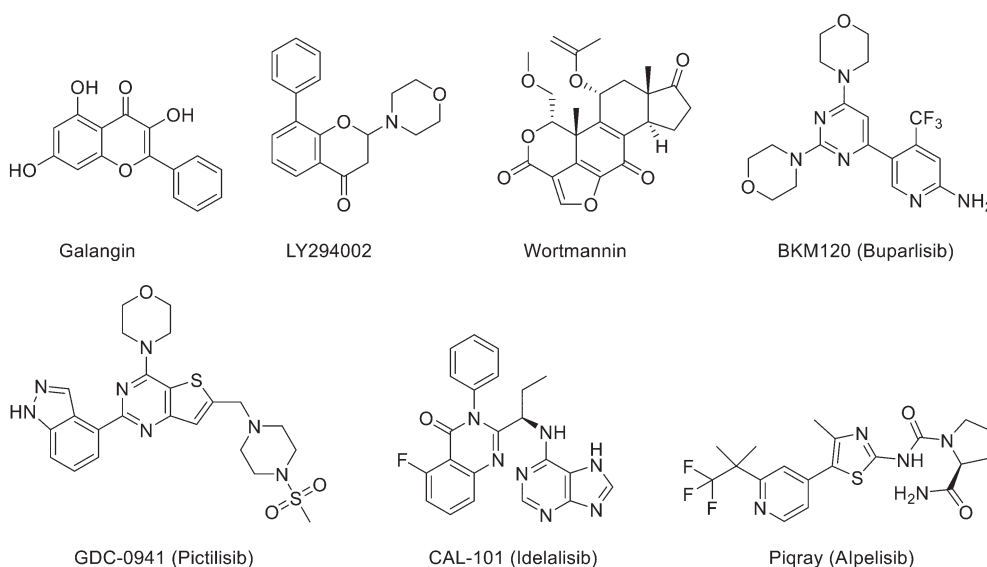
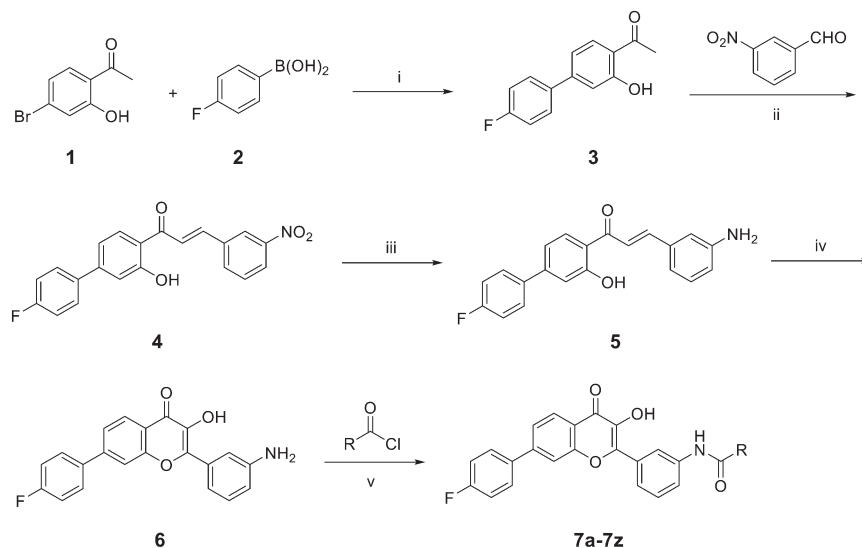


Fig. 1 The structure of PI3K/AKT pathway targeted regulatory agents.



Scheme 1 Synthetic route of target compounds. Reagents and conditions: (i) K_2CO_3 , $Pd(OAc)_2$, dioxane, 110 °C, 5 h; (ii) K_2CO_3 , MeOH, 50 °C, reflux, 16 h; (iii) $SnCl_2$, AcOH, $H_2O/MeOH$, 90 °C, 12 h; (iv) 30% H_2O_2 , NaOH, MeOH, 0–5 °C, rt, 10 h; (v) acetone, pyridine, rt, 3 h.

condensation in the presence of K_2CO_3 in MeOH to afford compound **4**. Reduction of the nitro in intermediate **4** by $SnCl_2$ produced the corresponding amino product **5** and it was subsequently cyclized under H_2O_2 and NaOH using methanol as a solvent to obtain intermediate **6**. Finally, flavonoid compound **6** was condensed with a series of acyl chlorides in acetone and pyridine to provide the target compounds **7a–7z**, which were characterized through nuclear magnetic resonance (NMR) and high-resolution mass spectrometry (HRMS).

2.2 Antiproliferative assay *in vitro*

All synthesized compounds (**7a–7z**) were evaluated for their *in vitro* antiproliferation activities against seven human cancer cell lines including MDA-MB-231 (human breast cancer cell line), MCF-7 (human breast cancer cell line), HCC1937 (human breast cancer cell line), A549 (human non-small cell lung cancer cell line), HepG2 (human hepatocellular liver carcinoma cell line), GTL-16 (human gastric cancer cell line), and HeLa (human cervical carcinoma cell line) through the Cell Counting Kit-8 (CCK8) assay. LY294002 and 5-fluorouracil (5-Fu) were used as positive controls.

As depicted in Table 1, many compounds exhibited good cytotoxicity against these seven cell lines manifesting as IC_{50} values that were much lower than that of the well-known antitumor cytotoxic drug 5-Fu, while the other control flavonoid LY294002 showed a relatively less efficient antiproliferation potency. Notably, some compounds had excellent specific antiproliferative activities on breast cancer related cell lines such as MDA-MB-231, MCF-7, and HCC1937. For instance, compounds **7d**, **7g**, **7r**, **7t**, and **7u** presented favorable antiproliferative effects against these

three cell lines with IC_{50} values ranging from 1.76 μM to 9.05 μM , all of which were superior to the positive control 5-Fu.

The most potent antiproliferation activity against the TNBC cell line MDA-MB-231 was obtained from compound **7t** whose R group at the 3'-position of the amide fragment was 6-chloro-3-pyridyl with an IC_{50} value of $1.76 \pm 0.91 \mu M$, which was nearly four times the potency of 5-Fu (IC_{50} value of $7.75 \pm 0.82 \mu M$). Compounds **7u** and **7m** whose R group was 3,5-difluorophenyl and 3-fluorophenyl, respectively, showed the second and third highest antiproliferative capabilities on MDA-MB-231 cells with IC_{50} values of $2.49 \pm 0.44 \mu M$ and $2.51 \pm 0.93 \mu M$, respectively. These results indicated that, for the cytotoxicity on MDA-MB-231 cells, a pyridyl substituent on the R group was preferred over a phenyl, and a fluorine-substituted phenyl moiety was better than other phenyl substituents. Besides its excellent cytotoxicity on MDA-MB-231, compound **7u** also displayed favorable antiproliferative capacity against MCF-7 and HCC1937 cells with IC_{50} values of $2.49 \pm 0.44 \mu M$ and $2.07 \pm 1.06 \mu M$, respectively. These results suggested that compound **7u** was not only the optimum compound with a comprehensive inhibitory effect on these breast cancer cells, but also the strongest cytotoxic agent against the TNBC cell line HCC1937 which exceeded the effectiveness of 5-Fu by ten-fold (IC_{50} : $25.94 \pm 1.12 \mu M$). Compound **7w** whose R group was 4-cyanophenyl exhibited the second powerful antiproliferation capability on HCC1937 (IC_{50} : $2.99 \pm 0.56 \mu M$) and gratifying proliferation inhibition activity on MCF-7, but a relatively reduced cytotoxicity against MDA-MB-231.

In addition, further investigations indicated that the 3,5 positions on the benzene ring in the R group being doubly substituted by fluorine was more favorable to enhance potent and broad-spectrum cytotoxicity against breast cancer cells compared to the mono-fluorophenyl or other mono-substituted phenyl substituted compounds. These

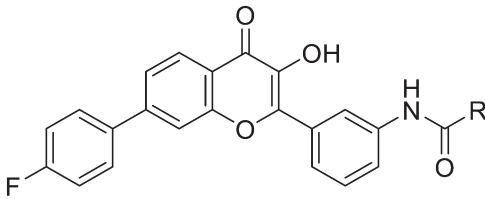
Table 1 Cytotoxicity of target compounds 7a–7z against MDA-MB-231, MCF-7, HCC1937, A549, HepG2 and GTL-16 cells *in vitro*

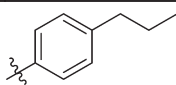
Compd.	R	IC ₅₀ ^a (mean ± SD μmol L ⁻¹)						
		MDA-MB-231	MCF-7	HCC1937	A549	Hep G2	GTL-16	HeLa
7a		7.24 ± 0.47	7.57 ± 0.27	10.76 ± 0.43	4.41 ± 0.83	10.14 ± 0.91	17.44 ± 1.10	5.63 ± 0.48
7b		16.02 ± 0.89	8.59 ± 0.78	14.23 ± 0.90	6.93 ± 0.55	9.28 ± 0.83	14.64 ± 1.39	5.35 ± 1.05
7c		16.52 ± 1.03	6.25 ± 0.64	5.49 ± 0.63	8.70 ± 1.03	8.42 ± 0.71	21.07 ± 1.84	4.82 ± 1.69
7d		4.35 ± 0.94	2.40 ± 0.61	7.11 ± 0.94	6.91 ± 0.32	2.32 ± 0.57	12.92 ± 1.08	6.19 ± 1.08
7e		12.80 ± 0.98	4.73 ± 0.71	4.03 ± 0.73	10.82 ± 0.66	11.01 ± 1.25	9.14 ± 0.87	3.67 ± 1.26
7f		11.17 ± 0.63	13.45 ± 0.41	6.98 ± 0.38	20.46 ± 0.74	26.35 ± 0.82	9.64 ± 0.60	10.73 ± 1.70
7g		5.11 ± 0.95	2.10 ± 0.86	9.05 ± 1.10	11.66 ± 0.74	14.51 ± 1.47	6.37 ± 0.91	14.07 ± 0.38
7h		4.91 ± 1.08	2.28 ± 0.62	9.90 ± 0.82	17.55 ± 0.99	19.39 ± 1.43	24.78 ± 1.29	11.86 ± 0.61
7i		29.39 ± 0.49	32.62 ± 0.99	7.35 ± 0.81	19.37 ± 0.93	42.70 ± 0.83	33.01 ± 1.76	17.35 ± 1.11
7j		24.93 ± 0.89	24.02 ± 0.69	8.63 ± 0.99	13.51 ± 0.98	13.89 ± 1.08	25.44 ± 0.86	9.74 ± 0.88
7k		9.16 ± 0.97	15.27 ± 0.51	18.89 ± 0.76	10.80 ± 0.35	9.95 ± 0.96	12.46 ± 1.76	5.65 ± 1.00
7l		2.84 ± 0.20	7.85 ± 1.13	8.03 ± 1.12	16.45 ± 0.77	13.49 ± 0.86	10.89 ± 1.11	6.65 ± 1.00
7m		2.51 ± 0.93	5.77 ± 0.90	6.59 ± 0.61	15.39 ± 0.94	15.48 ± 1.06	15.82 ± 1.40	8.78 ± 1.15

Table 1 (continued)

Compd.	R	IC ₅₀ ^a (mean ± SD μmol L ⁻¹)						
		MDA-MB-231	MCF-7	HCC1937	A549	Hep G2	GTL-16	HeLa
7n		9.07 ± 0.51	22.77 ± 1.08	13.24 ± 0.34	18.47 ± 0.99	20.62 ± 1.04	24.56 ± 1.36	21.01 ± 1.55
7o		NT	NT	NT	46.11 ± 1.06	>100	NT	NT
7p		7.44 ± 0.37	7.71 ± 1.01	5.42 ± 0.78	11.45 ± 0.83	9.54 ± 0.76	12.10 ± 0.92	18.86 ± 1.53
7q		17.56 ± 0.84	20.03 ± 1.01	24.45 ± 0.64	39.95 ± 1.25	45.33 ± 1.14	15.30 ± 1.62	16.09 ± 1.05
7r		4.04 ± 0.31	3.47 ± 1.08	6.25 ± 0.47	2.39 ± 0.41	23.47 ± 0.64	19.58 ± 1.44	2.70 ± 1.03
7s		11.94 ± 1.00	20.43 ± 1.50	4.86 ± 0.88	3.74 ± 0.35	13.37 ± 1.31	13.51 ± 1.36	5.54 ± 1.10
7t		1.76 ± 0.91	2.89 ± 0.86	7.55 ± 0.95	3.58 ± 0.62	4.61 ± 0.49	7.52 ± 0.94	4.08 ± 1.19
7u		2.44 ± 0.76	2.49 ± 0.44	2.07 ± 1.06	7.62 ± 1.10	4.96 ± 0.93	7.41 ± 0.87	3.38 ± 0.66
7v		NT	NT	NT	>100	>100	NT	NT
7w		11.60 ± 0.92	2.66 ± 1.02	2.99 ± 0.56	2.36 ± 0.45	7.11 ± 0.99	31.81 ± 1.04	23.30 ± 1.40
7x		14.73 ± 0.83	3.97 ± 0.36	5.64 ± 0.41	2.44 ± 0.55	1.86 ± 0.35	18.22 ± 0.89	12.34 ± 0.69
7y		63.24 ± 1.02	38.49 ± 0.94	44.08 ± 1.15	>100	88.48 ± 1.40	NT	>100

Table 1 (continued)



Compd.	R	IC ₅₀ ^a (mean ± SD μmol L ⁻¹)						
		MDA-MB-231	MCF-7	HCC1937	A549	Hep G2	GTL-16	HeLa
7z		32.18 ± 1.13	36.77 ± 1.23	15.35 ± 1.32	47.62 ± 1.20	51.52 ± 1.11	20.44 ± 1.16	8.79 ± 1.23
5-Fu ^b		7.75 ± 0.82	4.42 ± 0.89	25.94 ± 1.12	2.65 ± 0.12	2.88 ± 0.88	0.84 ± 0.19	1.94 ± 0.23
LY294002 ^b		31.76 ± 0.71	39.62 ± 1.80	37.84 ± 1.26	34.13 ± 1.53	30.86 ± 1.74	24.38 ± 1.06	16.97 ± 1.48

^a Antitumor activity was assayed by exposure to the substances for 72 h and is expressed as the concentration required to inhibit tumor cell proliferation by 50% (IC₅₀); values were the means of three replicates ± standard deviation (SD). ^b Used as a positive control.

conclusions were consistent with observations from compound **7g** bearing 2-methoxyphenyl in the R group. Compared to compounds **7t** and **7u**, compound **7g** only showed forceful proliferative inhibition on MCF-7 with an IC₅₀ value of 2.10 ± 0.86 μM, while obvious decreased antiproliferation effects on the other two TNBC cells, MDA-MB-231 and HCC1937, were afforded.

It was worth noting that different selectivities for wild-type *versus* mutant TNBC cells were obtained from compounds **7t** and **7w**. The antiproliferation on the wild TNBC cell line MDA-MB-231 of compound **7t** was superior to that of the mutant TNBC cell line HCC1937 (IC₅₀: 1.76 *vs.* 7.55 μM) and the selectivity ratio between the mutants and wild types was 1:4.29. In contrast, compound **7w** possessed preferred cytotoxicity on the mutant type than the wild type (IC₅₀: 11.60 *vs.* 2.99 μM) with a selectivity ratio of 3.88:1. Such observations were of great significance for the development of TNBC therapeutic drugs for different stages and types.

To our delight, some of the synthesized compounds also showed comparable cytotoxicity against non-small cell lung cancer A549 and hepatocellular carcinoma HepG2 cells to the positive control 5-Fu. For example, compound **7x** with an electron-withdrawing substituent 4-nitrophenyl on the R group possessed the most antiproliferative potency on HepG2 among all target compounds and its IC₅₀ value was 1.86 ± 0.35 μM which was superior to that of 5-Fu (IC₅₀ = 2.88 ± 0.88 μM). Moreover, a comparable cytotoxicity on A549 to that of 5-Fu was obtained from compound **7x** (IC₅₀: 2.44 ± 0.55 μM *vs.* 2.65 ± 0.12 μM). In addition to **7x**, compounds **7r** and **7w** also had almost equivalent antiproliferation activities against A549 cells to 5-Fu, whereas a slightly better proliferative inhibition effect on HepG2 cells was afforded by compound **7d** with an IC₅₀ value of 2.32 ± 0.57 μM.

A preliminary analysis of the structural characteristics affecting the specific antiproliferative ability against A549 and HepG2 cells revealed that substituents at the 4-position on the benzene ring in the R group exhibited a significant

influence. The nitro group was the best substituent and methyl or cyano moieties also achieved satisfactory outcomes. Meanwhile substituents with hydrogen or chain alkyl such as ethyl gave poor activities. Compared to 2- or 3-positions, substituents on the 4-position were preferred. Disubstituted derivatives of the benzene ring in the R group showed less efficient antiproliferation activities than 4-position substituted compounds. Moreover, replacement of phenyl with pyridyl in the R group displayed comparable cytotoxicity but pyrimidinyl substitution resulted in complete inactivation.

Nevertheless, the target compounds exhibited less efficient cytotoxicity on human cervical carcinoma HeLa cells. The IC₅₀ value of the best efficiency compound could be as low as 2.70 ± 1.03 μM, but was still slightly less effective than 5-Fu (IC₅₀ = 1.94 ± 0.23 μM). Unfortunately, the antiproliferative capability of the synthesized compounds against human gastric cancer GTL-16 cells was limited and all IC₅₀ values were much worse than that of 5-Fu. The most active compound only gave an IC₅₀ value of 6.37 μM, which was nearly eight-fold higher than that of 5-Fu (IC₅₀: 0.84 μM).

Taken together, due to the remarkable specific cytotoxicity of compound **7t**, combined with extremely limited clinical treatment options and drugs for TNBC, we selected it for further investigation in order to provide a basis for exploration of new candidates with a high therapeutic index.

2.3 Colony-forming assay of compound **7t**

To further explore the proliferation inhibitory effect on MDA-MB-231 cells of compound **7t**, a plate colony-forming assay was performed to determine its influence on the number and size of colony-forming cells and analyze the changes of colony-forming ability of MDA-MB-231 cells.

As described in Fig. 2, the number and size of MDA-MB-231 cells were inhibited dramatically by treatment with compound **7t** with the concentration increasing (0.25IC₅₀,

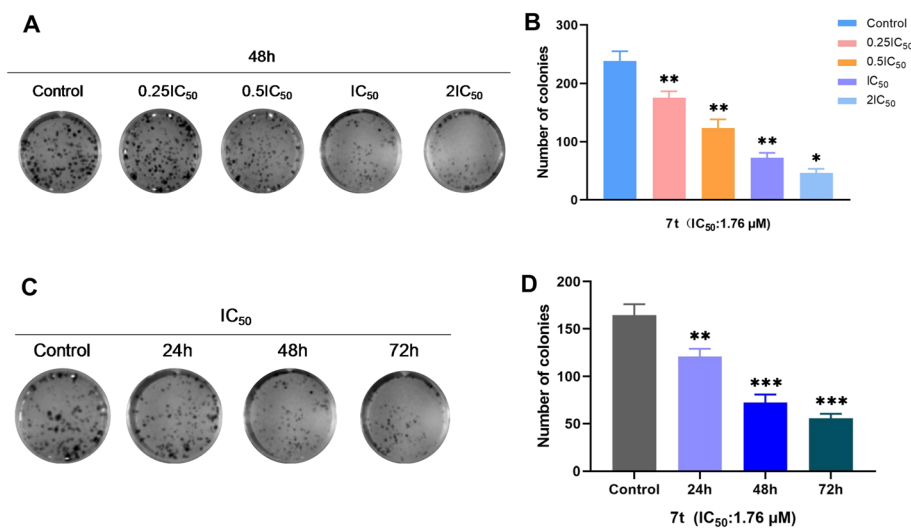


Fig. 2 (A and C) Effect of compound **7t** on colony-formation inhibition of MDA-MB-231 cells. (B and D) Numbers of colonies counted by image, $n = 3$. * $P < 0.05$, ** $P < 0.01$, *** $P < 0.001$ compared to the control.

0.5IC₅₀, IC₅₀ and 2IC₅₀) and time prolonging (24 h, 48 h and 72 h). It was indicated that compound **7t** had colony-formation inhibitory abilities on MDA-MB-231 cells in both a dose- and time-dependent manner.

2.4 Hoechst staining and flow cytometry assays of compound **7t**

To confirm whether the antiproliferation effect of compound **7t** on MDA-MB-231 cells was associated with induction of apoptosis, Hoechst staining and flow cytometry assays were carried out. According to the Hoechst staining image in Fig. 3A, with the increase in concentration of compound **7t** (0.5IC₅₀, IC₅₀, 2IC₅₀), a growing number of morphological changes from MDA-MB-231 cells occurred obviously such as chromatin concentration and margination, half-moon, loop and ellipse shaped fragment formation, and emergence of apoptotic bodies; it further showed that the floating cells with fluorescent spots grew dramatically. Thus, it was suggested that compound **7t** could significantly induce apoptosis of MDA-MB-231 cells in a concentration-dependent manner as summarized in Fig. 3B.

On the basis of the cell cycle assay depicted in Fig. 3C and D, the proportion of the G₀/G₁ phase of MDA-MB-231 cells elevated obviously with increasing concentration (0.5IC₅₀, IC₅₀ and 2IC₅₀) in each dose group administrated with compound **7t** after 48 h compared with the blank group. On the contrary, a dramatic decrease in the proportion of the S-phase combined with a slight reduction in the proportion of the G₂/M-phase of MDA-MB-231 cells was observed, indicating that compound **7t** inhibited the growth cycle transition of MDA-MB-231 cells and blocked the cell growth cycle at the G₀/G₁ phase.

Furthermore, the apoptosis graphic of MDA-MB-231 cells was afforded by flow cytometry utilizing the Annexin V-FITC/PI double staining method. In the light of the statistical cell proportion illustrated in Fig. 3E and F, compound **7t** strongly

induced the apoptosis of MDA-MB-231 cells and the overall apoptosis rate raised gradually with increasing concentration (0.5IC₅₀, IC₅₀, 1.25IC₅₀, 2IC₅₀ and 4IC₅₀). None of the evident early apoptotic cells were observed under the concentrations of 0.5IC₅₀ while the proportions of early and late apoptotic cells gradually rose when the concentrations were greater than IC₅₀ (the early/late apoptosis ratios were 46.96%/3.81% and 68.96%/14.4% for concentrations of IC₅₀ and 2IC₅₀, respectively). Such observations demonstrated that compound **7t** induced a concentration-dependent apoptosis induction on MDA-MB-231 cells.

2.5 Transwell simulated cell invasion and wound-healing assays of compound **7t**

Owing to the invasion of cancer cells which is a process that is inextricably linked to cell metastasis, a Transwell simulated cell invasion assay was applied to examine the effect of compound **7t** on the invasive ability of MDA-MB-231 cells at different concentrations. As shown in Fig. 4A and B, the number of cells crossing the microporous membrane decreased gradually at the concentrations of 0.5IC₅₀, IC₅₀, and 2IC₅₀, indicating that compound **7t** displayed significant potency to suppress the invasion capability of MDA-MB-231 cells in a concentration-dependent manner.

As the metastasis of cancer cells is related to their migration ability, a wound healing assay was conducted to probe the inhibitory effect of compound **7t** on the migration of MDA-MB-231 cells at different concentrations and times. The corresponding results could be determined by measurement of the scratch distance and statistics of scratch mobility. As demonstrated in Fig. 4C and D, the scratch healing speed slowed down and the movement migration ability was affected *via* administration of compound **7t** at the concentration of 0.5IC₅₀ after 12 h compared with the blank group. Subsequently, the relative migration rate of MDA-MB-

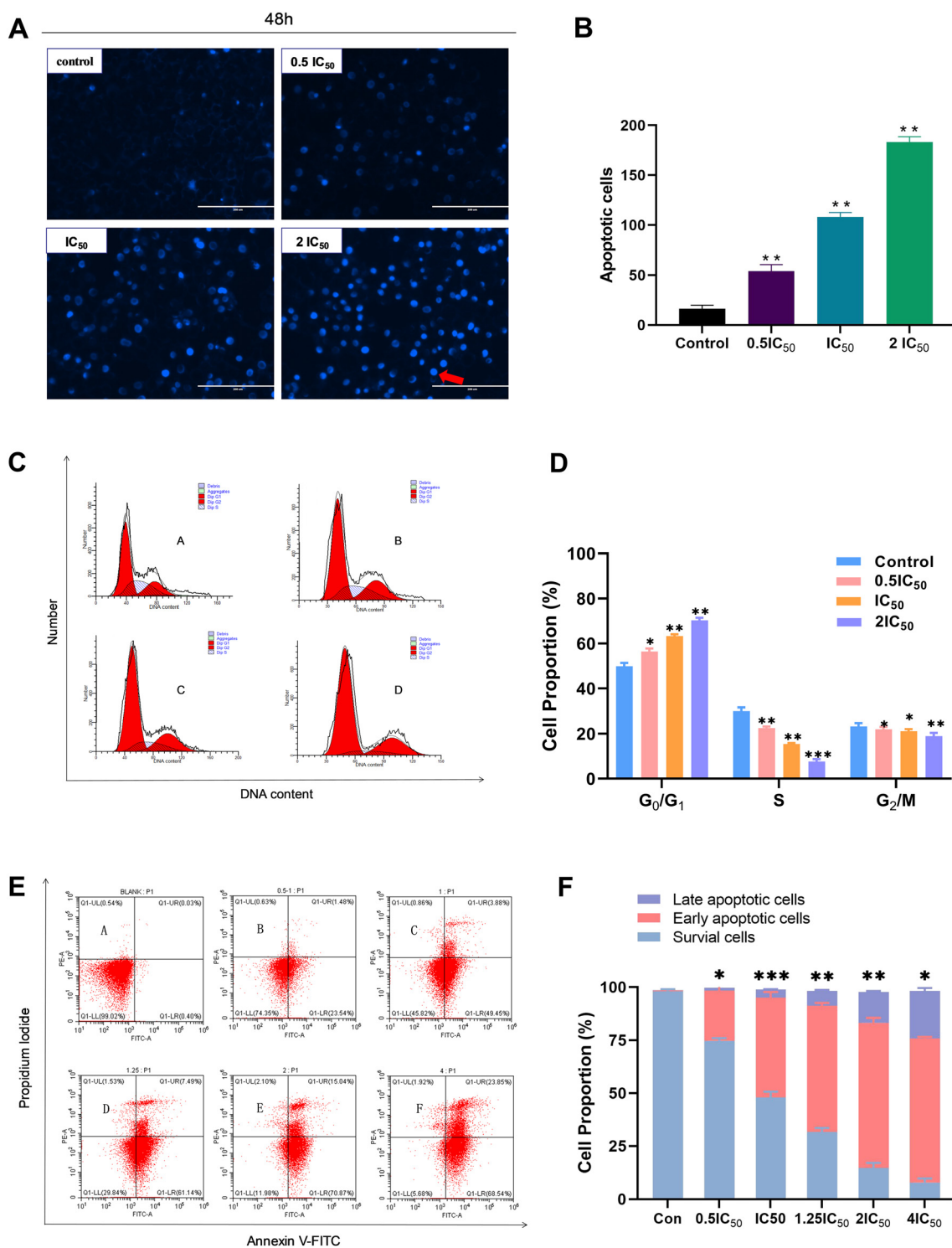


Fig. 3 The effect of compound **7t** on MDA-MB-231 cell apoptosis and the cell cycle. MDA-MB-231 cells were treated with the indicated concentrations of **7t** for 48 h, and apoptotic cells were detected by Hoechst 33342 staining and flow cytometry, respectively. All data represent the mean \pm SD, $n = 3$, $*P < 0.05$, $**P < 0.01$, $***P < 0.001$ compared to the control. (A) The effect of compound **7t** on apoptosis of MDA-MB-231 cells by Hoechst staining. (B) Statistical apoptosis cell proportion of MDA-MB-231 with different dose concentrations of compound **7t**. (C) The effect of compound **7t** on the cell cycle in MDA-MB-231 cells obtained through the flow cytometry assay. (D) The flow cytometry data analysis as a means to measure the percentages of G₀/G₁, S, and G₂/M. (E) Effect of compound **7t** on apoptosis of MDA-MB-231 cells measured through the Annexin V-FITC/PI assay. (F) The flow cytometry data analysis as a means to obtain the percentages of survival cells, early and late apoptotic cells.

231 cells abated obviously with increasing dose concentrations and the relative migration rates were 64.13%,

42.32%, 35.41% and 23.11% at concentrations of 0, 0.5IC₅₀, IC₅₀, and 2IC₅₀, respectively after 48 h, which meant that the

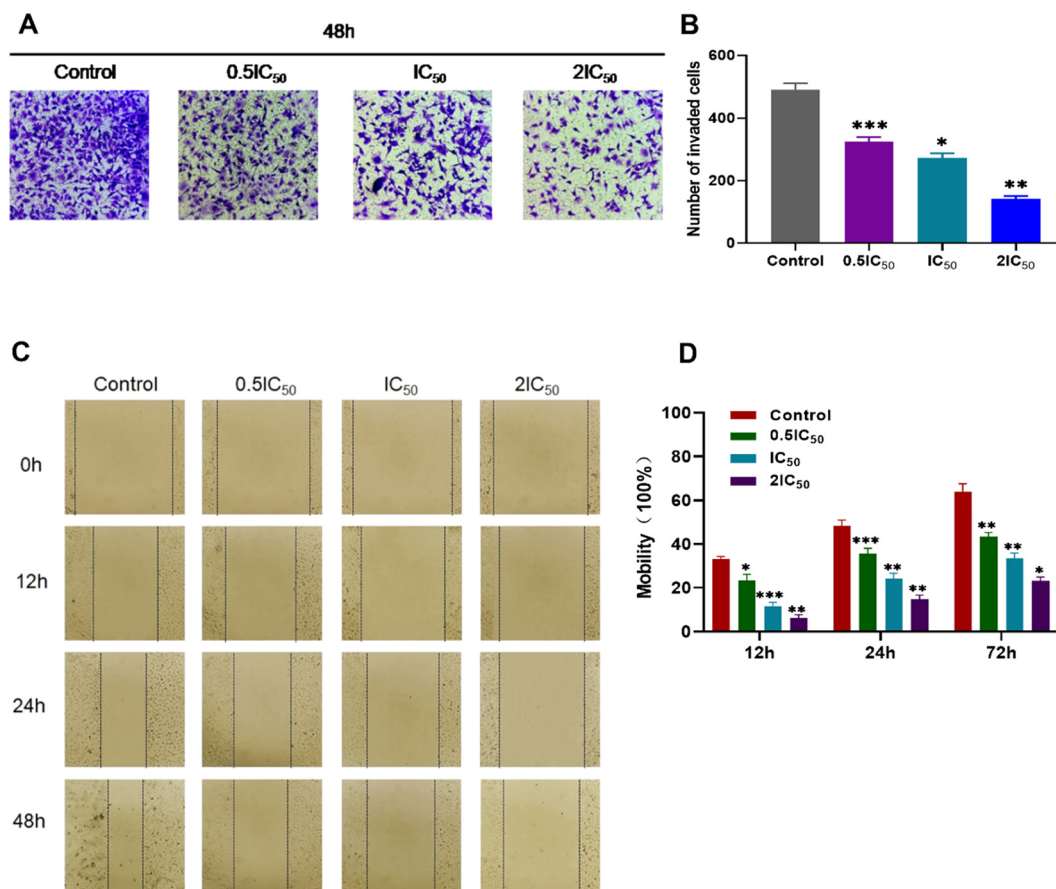


Fig. 4 The effect of compound **7t** on MDA-MB-231 cell invasion and migration. All data represent the mean \pm SD, $n = 3$, * $P < 0.05$, ** $P < 0.01$, *** $P < 0.001$ compared to the control. (A) The effect of compound **7t** on Transwell cell invasion assays. (B) Statistical number of invaded MDA-MB-231 cells with treatment with compound **7t** at different dose concentrations. (C) The wound healing assay for compound **7t** on MDA-MB-231 cells. (D) Statistics of scratch mobility from MDA-MB-231 cells with compound **7t** at different dose concentrations.

motility of MDA-MB-231 cells was significantly inhibited by compound **7t** at high lever concentrations. All these outcomes suggested that compound **7t** suppressed the migration capacity of MDA-MB-231 cells in a concentration-dependent manner.

2.6 Western blot assay in MDA-MB-231 cells of compound **7t**

With the aim of making a further effort on the mechanism exploration of the antiproliferation potency against MDA-MB-231 cells of compound **7t**, a Western blot assay was employed to discuss its influence on the PI3K/AKT signaling pathway namely the relevant protein expression of PI3K, p-PI3K, AKT, p-AKT, and PTEN, and apoptosis related protein expression, such as caspase-3, Bcl-2, and Bax. As illustrated in Fig. 5, by treatment with compound **7t** on MDA-MB-231 cells at concentrations of 1 μ M, 5 μ M, and 10 μ M for 48 h, respectively, the production of phosphorylated PI3K and phosphorylated AKT was inhibited in a concentration-dependent manner. The expression of tumor suppressor gene PTEN was up-regulated. Besides, the downstream anti-apoptotic protein Bcl-2 was down-regulated and the pro-apoptotic protein Bax as well as the apoptotic execution

protein caspase-3 was up-regulated, and the apoptosis of MDA-MB-231 cells was thereby induced. Consequently, compound **7t** possessed excellent antiproliferation performance *via* inhibition of the PI3K/AKT signaling pathway and induction of apoptosis as it could not only suppress the phosphorylation of PI3K and AKT to inactivate downstream targets, but also regulate cell death through endogenous pathways.

2.7 Modeling of compound **7t** on PI3K α

A molecular docking study was carried out to predict the possible binding mode between compound **7t** and PI3K α (PDB: 4tv3), which could be responsible for the potent antiproliferation activity. The molecular simulation protocol was initially validated by re-docking of the co-crystallized ligand into the binding sites of PI3K α and the reliability was verified by a high similarity value between the re-docked and original ligand poses from the Sybyl-X 2.1 software. As shown in Fig. 6, compound **7t** can perfectly be docked into the active site of 4tv3 as evidenced by satisfactory scoring functions such as total-score and c-score. The critical hydrogen bond of carbonyl and hydroxyl groups with Val851 was formed similar

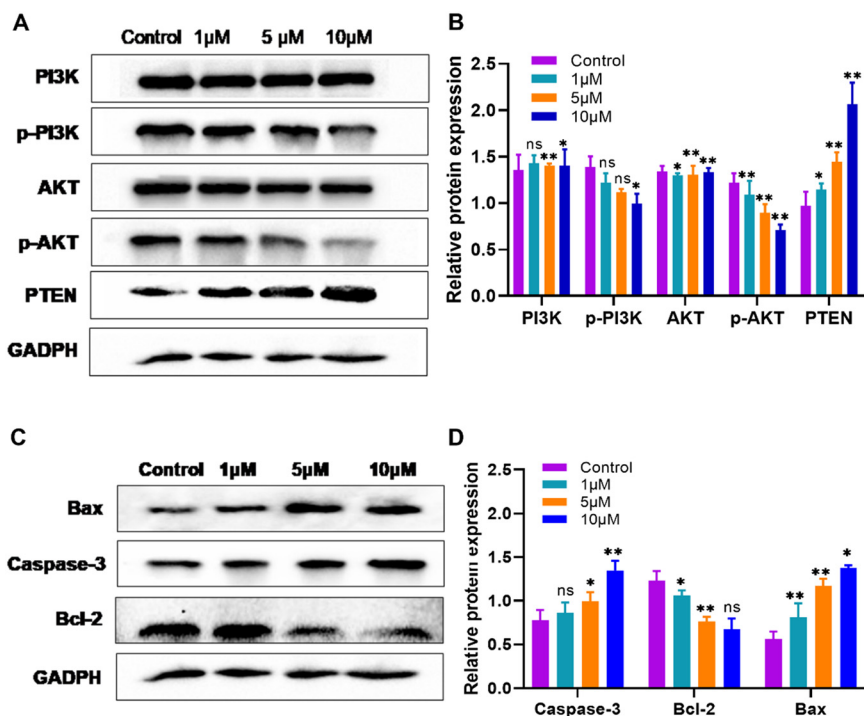


Fig. 5 Western blot assay of MDA-MB-231 treated with compound 7t. (A) Western blot analysis of proteins involved in the PI3K/AKT signaling pathway. (B) Regulation statistics on the expression of PI3K/AKT signaling pathway-related proteins in MDA-MB-231 cells. (C) Western blot analysis of apoptosis-associated proteins. (D) Regulation statistics on the expression of apoptosis-related proteins in MDA-MB-231 cells.

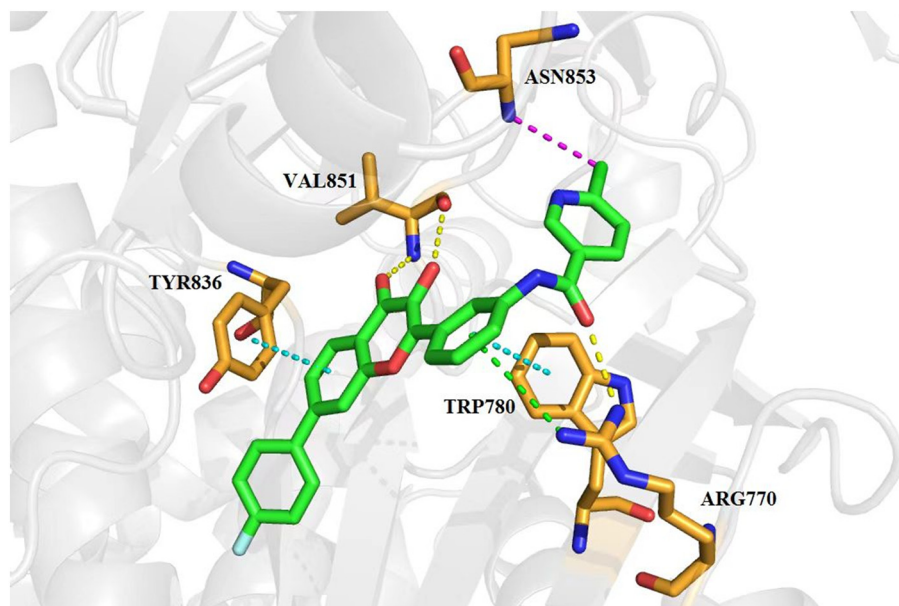


Fig. 6 Binding mode of compound 7t in the active site of PI3K α obtained from molecular docking. 7t was represented in stick colored with green carbon, red oxygen and blue nitrogen respectively, while the surrounding key residues were depicted in stick with brown carbon, red oxygen and blue nitrogen. Hydrogen and halogen bonds were shown in dashed lines colored yellow and purple respectively. π - π stacking and π -cation interactions were described in dotted lines colored cyan and green respectively.

to LY294002. The carbonyl group in the amide fragment formed another key hydrogen bond with residue Arg770. In addition, the two phenyl groups of the flavonol scaffold

formed π - π stacking interaction with Tyr836 and Trp780, respectively. The benzene ring on the 2-position with guanidyl of the Arg770 residue produced an important π -

cation interaction. Furthermore, the chlorine atom on the pyridine ring formed a halogen bond with residue Asn853. All these interactions may contribute to its significant antiproliferative potency.

3. Conclusions

In summary, a series of novel flavonoid-based amide compounds were synthesized and evaluated for their *in vitro* anticancer bioactivities against seven tumor cell lines. Among them, compounds **7t** and **7u** presented significant specific antiproliferation activities on breast cancer cell lines. Compound **7u** was the strongest cytotoxic agent against mutant type TNBC cell HCC1937 with an IC₅₀ value of 2.07 ± 1.06 μM which was exceeded the positive control 5-Fu by ten-fold. Compound **7t** possessed the most antiproliferative ability against wild type TNBC cell MDA-MB-231 with an IC₅₀ value of 1.76 ± 0.91 μM, nearly four times the potency of 5-Fu. In addition, compound **7t** presented inhibitory ability on clonal-formation, migration and invasion of MDA-MB-231 cells. Further cell-based mechanistic studies indicated that compound **7t** caused cell cycle arrest of MDA-MB-231 cells in a dose dependent manner at the G₀/G₁ phase and induced apoptosis. Moreover, the western blot assay demonstrated that compound **7t** could down-regulate the expression of p-PI3K, p-AKT, and Bcl-2 and up-regulate the expression of PTEN, Bax, and caspase-3 so as to inhibit the PI3K/AKT pathway from achieving its significant antiproliferative effects. Molecular docking simulation also showed a possible binding mode of compound **7t** with PI3Kα. Overall, the obtained compounds **7t** and **7u** were eligible as potential regulators of the PI3K/AKT pathway to be further developed and provided a basis for TNBC curative candidates.

4. Experimental

4.1 General information

The ¹H NMR and ¹³C NMR spectra were recorded using TMS as the internal standard on a Bruker Advance III 400 spectrometer (Bruker, Switzerland) at 400 MHz and 101 MHz in either CDCl₃ or DMSO-*d*₆. Chemical shifts (δ) were referenced to TMS as an internal standard (¹H NMR, ¹³C NMR). Coupling constants are given in Hz. High-resolution mass (HRMS) spectra were obtained with a Thermo-DFS mass spectrometer (ThermoFisher Scientific, USA). Reaction progress was monitored using analytical thin layer chromatography (TLC) on precoated silica gel GF₂₅₄ (Qingdao Haiyang Chemical Plant, Qingdao, China) plates, and the spots were detected under UV light (254 nm). Flash column chromatography was performed with silica gel (200–300 mesh) purchased from Qingdao Haiyang Chemical Co. Ltd. All other chemical materials were obtained from commercial suppliers and were used without further purification.

All cancer cell lines MDA-MB-231, MCF-7, HCC1937, A549, HepG2, GTL-16, and Hela were purchased from iCell Bioscience Inc, Shanghai. Biological materials including

plasma, fetal bovine serum (FBS), DMEM medium and pancreatin were purchased from Shanghai Beyotime Biotechnology Co., Ltd. Cell Counting Kit-8, annexin V-APC/PI apoptosis analysis kits, and flow cytometry kits for apoptosis were purchased from Jiangsu KeyGEN BioTECH Co., Ltd. Penicillin–streptomycin liquid, Hoechst 33258 staining solution and phosphate buffer saline (PBS) were purchased from Hangzhou Genom Biotechnology Co., Ltd.

4.2 Synthesis of compound 3

4-Bromo-2-hydroxyacetophenone (4.0 g, 18.6 mmol), *p*-fluorophenylboronic acid (3.9 g, 27.9 mmol), palladium acetate (0.42 g, 1.86 mmol), and potassium carbonate (7.7 g, 55.8 mmol) were added sequentially to a 100 mL flask and charged with nitrogen. 1,4-Dioxane (20 ml) and water (4 ml) were slowly injected into the flask *via* a syringe, and the reaction mixture was stirred at 110 °C with reflux for 5 h. After completion monitored by thin-layer chromatography (TLC), the mixture was acidified to pH 6–7 with an aqueous solution of acetic acid. The mixture solution was then filtered and the filtrate was extracted with EtOAc. The combined organic layers were dried over Na₂SO₄ and the solvent was evaporated under vacuum. The obtained crude product was purified by flash chromatography on silica gel (*V*_{ethyl acetate}/*V*_{petroleum ether} = 1/40) to give 2.623 g of product as a white solid. Yield 65%. ¹H NMR (400 MHz, DMSO-*d*₆) δ 12.13 (s, 1H), 7.94 (d, *J* = 8.3 Hz, 1H), 7.80–7.74 (m, 2H), 7.33–7.27 (m, 2H), 7.24 (dd, *J* = 8.2, 1.9 Hz, 1H), 7.21 (d, *J* = 1.7 Hz, 1H), 2.65 (s, 3H); ¹³C NMR (101 MHz, DMSO-*d*₆) δ 204.68, 164.34, 161.85, 147.05, 135.43, 132.64, 129.73, 129.65, 119.58, 118.06, 116.52, 116.30, 115.59, 27.94; HR-ESI-MS calcd for C₁₄H₁₁FO₂ [M + H]⁺ 231.0743; found 231.0813.

4.3 Synthesis of compound 4

Compound 3 (2.0 g, 8.7 mmol) and 3-nitrobenzaldehyde (1.3 g, 8.7 mmol) were dissolved in methanol (20 mL) and KOH (2.4 g, 43.5 mmol) was added subsequently. The reaction mixture was then stirred at 50 °C for 16 h. After completion monitored by TLC, the reaction mixture was acidified to pH 6–7 with an aqueous solution of acetic acid to allow the yellow solid to precipitate. The solid was collected by filtration and the obtained crude product was purified by flash chromatography on silica gel (*V*_{ethyl acetate}/*V*_{petroleum ether} = 1/15) to give 1.16 g of product as a yellow solid. Yield 60%. ¹H NMR (400 MHz, DMSO-*d*₆) δ 8.72 (t, *J* = 1.9 Hz, 1H), 8.33 (d, *J* = 8.5 Hz, 1H), 8.28 (d, *J* = 7.8 Hz, 1H), 8.23–8.20 (m, 1H), 8.20–8.17 (m, 1H), 7.87 (d, *J* = 15.6 Hz, 1H), 7.78–7.74 (m, 2H), 7.70–7.66 (m, 1H), 7.26 (d, *J* = 8.9 Hz, 2H), 7.23 (d, *J* = 1.6 Hz, 1H), 7.20 (d, *J* = 1.8 Hz, 1H); ¹³C NMR (101 MHz, DMSO-*d*₆) δ 193.4, 163.0, 161.97, 148.9, 147.4, 142.6, 136.9, 135.9, 135.3, 132.4, 130.9, 129.9, 129.8, 125.5, 125.0, 123.8, 120.0, 118.1, 116.6, 116.4, 115.8; HR-ESI-MS calcd for C₂₁H₁₄FNO₄ [M + H]⁺ 364.0907; found 364.0966.

4.4 Synthesis of compound 5

To a solution of compound 4 (2.0 g, 5.5 mmol) in methanol (20 mL) were added SnCl₂ (4.2 g, 22.0 mmol) and acetic acid (5 mL) sequentially. The suspension solution was reacted at 90 °C with reflux overnight. After completion monitored by TLC, the reaction mixture was filtered and the filtrate was then diluted with water and extracted with CH₂Cl₂. The combined organic layers were washed with brine and dried over Na₂SO₄. The crude product was obtained through removing the solvent under vacuum and further purified by flash chromatography on silica gel (*V*_{ethyl acetate}/*V*_{petroleum ether} = 1/4) to give 1.43 g of product as a yellow solid. Yield 80%. ¹H NMR (400 MHz, DMSO-*d*₆) δ 8.23 (d, *J* = 8.3 Hz, 1H), 7.85 (d, *J* = 15.5 Hz, 1H), 7.80–7.76 (m, 2H), 7.67 (d, *J* = 15.4 Hz, 1H), 7.30 (s, 1H), 7.10 (t, *J* = 7.7 Hz, 1H), 7.05 (dt, *J* = 7.5, 1.1 Hz, 1H), 6.98 (t, *J* = 1.9 Hz, 1H), 6.67 (ddd, *J* = 7.8, 2.2, 1.2 Hz, 1H), 5.21 (s, 2H); ¹³C NMR (101 MHz, DMSO-*d*₆) δ 193.5, 164.4, 162.9, 161.9, 149.7, 147.0, 146.5, 135.5, 135.4, 131.9, 130.0, 129.8, 129.7, 121.1, 120.1, 118.1, 117.5, 116.6, 116.3, 115.8, 114.6; HR-ESI-MS calcd for C₂₁H₁₆FNO₂ [M + H]⁺ 334.1165; found 334.1233.

4.5 Synthesis of compound 6

To a mixture of compound 5 (1.0 g, 3.0 mmol) and NaOH (1.2 g, 30.0 mmol) in methanol/water mixed solvents (*V*_{methanol}/*V*_{water} = 4/1) was slowly added 30% hydrogen peroxide dropwise (6 mL) at 0–4 °C. The reaction mixture was then stirred at the same temperature for 16 h. After completion monitored by TLC, the mixture was acidified to pH 6–7 with an aqueous solution of hydrochloric acid to allow the yellow solid to precipitate. The solid was collected by filtration and the obtained crude product was purified by flash chromatography on silica gel (*V*_{ethyl acetate}/*V*_{petroleum ether} = 1/3) to give 0.58 g of product as a yellow solid. Yield 70%. ¹H NMR (400 MHz, DMSO-*d*₆) δ 8.31 (d, *J* = 8.4 Hz, 1H), 8.13 (d, *J* = 1.5 Hz, 1H), 8.07–8.03 (m, 2H), 7.91 (dd, *J* = 8.4, 1.6 Hz, 1H), 7.65 (t, *J* = 1.9 Hz, 1H), 7.59–7.56 (m, 1H), 7.54–7.49 (m, 2H), 7.36 (t, *J* = 7.9 Hz, 1H), 6.87 (ddd, *J* = 7.8, 2.2, 0.8 Hz, 1H), 5.46 (s, 2H); ¹³C NMR (101 MHz, DMSO-*d*₆) δ 173.3, 164.4, 161.9, 155.4, 149.2, 146.8, 144.5, 139.8, 135.2, 132.4, 129.9, 129.4, 126.0, 123.6, 120.6, 116.7, 116.4, 116.2, 116.1, 116.0, 113.4; HR-ESI-MS calcd for C₂₁H₁₄FNO₃ [M + H]⁺ 348.0958; found 348.1026.

4.6 General procedures for the preparation of 7a–7z

To a solution of compound 6 (0.5 g, 1.5 mmol) and pyridine (0.25 mL) in acetone (20 mL) were added the corresponding benzoyl chloride analogs (2.6 mmol) dropwise in an ice bath. The reaction mixture was then warm to room temperature and stirred for another 12 h. After completion monitored by TLC, the reaction solution was diluted with distilled water and extracted with CH₂Cl₂. The combined organic layers were washed with brine and dried over Na₂SO₄. Removing the solvent under vacuum afforded the crude product which was purified by flash chromatography on silica gel (*V*_{ethyl acetate}/

*V*_{petroleum ether} = 1:5) to give the corresponding target compounds 7a–7z.

4.6.1 2-Fluoro-*N*-(3-(7-(4-fluorophenyl)-3-hydroxy-4-oxo-4H-chromen-2-yl)phenyl)benzamide (7a). Light yellow solid. Yield 56%. Mp 224.6–226.1 °C. ¹H NMR (400 MHz, DMSO-*d*₆) δ 10.65 (s, 1H), 9.70 (s, 1H), 8.57 (s, 1H), 8.13 (d, *J* = 8.4 Hz, 1H), 7.97–7.93 (m, 2H), 7.88 (d, *J* = 2.0 Hz, 1H), 7.87 (d, *J* = 3.5 Hz, 1H), 7.85 (d, *J* = 5.4 Hz, 1H), 7.74 (dd, *J* = 8.4, 1.7 Hz, 1H), 7.67 (td, *J* = 7.6, 1.7 Hz, 1H), 7.60–7.54 (m, 1H), 7.54–7.50 (m, 1H), 7.37–7.33 (m, 1H), 7.33 (t, *J* = 2.3 Hz, 1H), 7.31 (d, *J* = 2.4 Hz, 1H), 7.31–7.28 (m, 1H); ¹³C NMR (101 MHz, DMSO-*d*₆) δ 173.2, 162.7, 159.4, 155.4, 145.6, 144.8, 140.0, 139.6, 135.2, 133.1, 132.3, 130.5, 130.0, 129.9, 129.5, 127.1, 126.1, 125.5, 125.4, 125.1, 123.8, 121.9, 121.9, 120.7, 119.7, 116.7, 116.5, 116.4; HR-ESI-MS calcd for C₂₈H₁₇F₂NO₄ [M + H]⁺ 470.1126; found 470.1196.

4.6.2 4-Fluoro-*N*-(3-(7-(4-fluorophenyl)-3-hydroxy-4-oxo-4H-chromen-2-yl)phenyl)benzamide (7b). Light yellow solid. Yield 58%. Mp 260.8–261.3 °C. ¹H NMR (400 MHz, DMSO-*d*₆) δ 10.62 (d, *J* = 20.0 Hz, 1H), 9.72 (s, 1H), 8.64 (dt, *J* = 9.4, 1.8 Hz, 1H), 8.26 (dd, *J* = 8.8, 5.5 Hz, 1H), 8.19–8.12 (m, 2H), 8.12–8.05 (m, 2H), 7.94 (d, *J* = 3.7 Hz, 1H), 7.93 (s, 1H), 7.92–7.89 (m, 1H), 7.55 (td, *J* = 8.0, 3.9 Hz, 1H), 7.42–7.38 (m, 2H), 7.37 (s, 1H), 7.37–7.32 (m, 2H); ¹³C NMR (101 MHz, DMSO-*d*₆) δ 173.2, 171.3, 165.1, 162.9, 156.6, 156.1, 155.5, 145.8, 144.7, 140.2, 139.9, 139.7, 133.8, 132.2, 131.1, 131.0, 130.0, 129.9, 122.1, 120.7, 116.7, 116.5, 116.5, 116.0, 116.0, 115.8, 115.8, 100.0; HR-ESI-MS calcd for C₂₈H₁₇F₂NO₄ [M + H]⁺ 470.1126; found 470.1181.

4.6.3 *N*-(3-(7-(4-fluorophenyl)-3-hydroxy-4-oxo-4H-chromen-2-yl)phenyl)-4-methoxy-benzamide (7c). Light yellow solid. Yield 65%. Mp 278.8–279.9 °C. ¹H NMR (400 MHz, DMSO-*d*₆) δ 10.32 (s, 1H), 9.62 (s, 1H), 8.57 (s, 1H), 8.10 (d, *J* = 8.3 Hz, 1H), 7.97 (s, 1H), 7.95 (s, 1H), 7.91 (d, *J* = 7.3 Hz, 1H), 7.87 (s, 1H), 7.85 (s, 1H), 7.83 (s, 1H), 7.72 (d, *J* = 8.1 Hz, 1H), 7.47 (t, *J* = 8.0 Hz, 1H), 7.29 (t, *J* = 8.6 Hz, 2H), 7.00 (d, *J* = 8.8 Hz, 2H), 3.77 (s, 3H); ¹³C NMR (101 MHz, DMSO-*d*₆) δ 173.2, 165.6, 162.5, 155.5, 145.9, 144.7, 143.4, 140.0, 139.9, 135.2, 132.1, 130.3, 130.0, 129.9, 129.2, 127.2, 126.1, 123.8, 123.6, 122.8, 120.7, 120.4, 116.70, 116.5, 116.3, 114.1, 56.0; HR-ESI-MS calcd for C₂₉H₂₀FNO₅ [M + H]⁺ 482.1326; found 482.1382.

4.6.4 *N*-(3-(7-(4-fluorophenyl)-3-hydroxy-4-oxo-4H-chromen-2-yl)phenyl)-4-methylbenzamide (7d). Light yellow solid. Yield 60%. Mp 274.5–275.0 °C. ¹H NMR (400 MHz, DMSO-*d*₆) δ 10.44 (s, 1H), 9.69 (s, 1H), 8.64 (s, 1H), 8.16 (d, *J* = 8.4 Hz, 1H), 8.00 (s, 1H), 7.98 (d, *J* = 8.2 Hz, 1H), 7.94 (s, 1H), 7.92 (s, 1H), 7.91–7.86 (m, 2H), 7.80–7.75 (m, 1H), 7.53 (t, *J* = 8.0 Hz, 1H), 7.37 (s, 1H), 7.35 (s, 2H), 7.33 (s, 1H), 2.38 (s, 3H); ¹³C NMR (101 MHz, DMSO-*d*₆) δ 173.2, 166.1, 161.9, 155.5, 145.8, 144.7, 142.3, 139.9, 139.9, 135.1, 135.1, 132.3, 132.1, 130.0, 129.9, 129.5, 129.2, 128.3, 126.1, 123.7, 122.8, 120.7, 120.4, 116.7, 116.5, 116.2, 21.6; HR-ESI-MS calcd for C₂₉H₂₀FNO₄ [M + H]⁺ 466.1376; found 466.1440.

4.6.5 4-Chloro-*N*-(3-(7-(4-fluorophenyl)-3-hydroxy-4-oxo-4H-chromen-2-yl)phenyl)benzamide (7e). Light yellow solid. Yield 70%. Mp 238.3–239.3 °C. ¹H NMR (400 MHz, DMSO-*d*₆)

δ 10.43 (s, 1H), 9.58 (s, 1H), 8.47 (s, 1H), 8.02 (d, J = 8.4 Hz, 1H), 7.89 (d, J = 1.8 Hz, 1H), 7.87 (s, 1H), 7.86 (s, 1H), 7.85 (d, J = 5.0 Hz, 1H), 7.77 (s, 1H), 7.76 (s, 1H), 7.74 (s, 1H), 7.64 (dd, J = 8.4, 1.5 Hz, 1H), 7.49–7.46 (m, 2H), 7.41 (t, J = 8.0 Hz, 1H), 7.21 (t, J = 8.8 Hz, 2H); ^{13}C NMR (101 MHz, DMSO- d_6) δ 173.3, 165.2, 162.0, 155.5, 145.7, 144.8, 139.9, 139.6, 137.1, 135.1, 133.9, 132.2, 130.2, 130.2, 130.0, 129.9, 129.4, 129.0, 126.1, 124.0, 123.8, 122.8, 120.7, 120.5, 116.7, 116.5, 116.2; HR-ESI-MS calcd for $\text{C}_{28}\text{H}_{17}\text{ClFNO}_4$ $[\text{M} + \text{H}]^+$ 486.0830; found 486.0888.

4.6.6 2,4-Difluoro-*N*-(3-(7-(4-fluorophenyl)-3-hydroxy-4-oxo-4*H*-chromen-2-yl)phenyl)benzamide (7f). Light yellow solid. Yield 69%. Mp 244.4–245.3 °C. ^1H NMR (400 MHz, DMSO- d_6) δ 10.73 (d, J = 17.7 Hz, 1H), 9.73 (s, 1H), 8.58 (s, 1H), 8.15 (dd, J = 8.4, 1.9 Hz, 1H), 7.99 (s, 1H), 7.98–7.96 (m, 1H), 7.92–7.90 (m, 1H), 7.89 (s, 1H), 7.88 (s, 1H), 7.82–7.78 (m, 1H), 7.78–7.75 (m, 1H), 7.55 (t, J = 8.1 Hz, 1H), 7.46–7.40 (m, 1H), 7.35 (t, J = 8.8 Hz, 2H), 7.23 (td, J = 8.9, 2.6 Hz, 1H); ^{13}C NMR (101 MHz, DMSO- d_6) δ 173.2, 162.7, 162.0, 155.5, 145.6, 144.8, 140.0, 139.5, 135.2, 135.1, 133.6, 132.3, 130.0, 129.9, 129.5, 126.9, 126.1, 123.9, 123.8, 121.9, 120.7, 119.8, 116.7, 116.5, 116.2, 112.5, 112.2, 105.2; HR-ESI-MS calcd for $\text{C}_{28}\text{H}_{16}\text{F}_3\text{NO}_4$ $[\text{M} + \text{H}]^+$ 488.1031; found 488.1104.

4.6.7 *N*-(3-(7-(4-Fluorophenyl)-3-hydroxy-4-oxo-4*H*-chromen-2-yl)phenyl)-2-methoxybenzamide (7g). Light yellow solid. Yield 69%. Mp 218.9–219.7 °C. ^1H NMR (400 MHz, DMSO- d_6) δ 10.36 (s, 1H), 9.68 (s, 1H), 8.62 (s, 1H), 8.16 (d, J = 8.4 Hz, 1H), 7.99 (d, J = 1.5 Hz, 1H), 7.96 (dt, J = 8.0, 1.3 Hz, 1H), 7.92–7.90 (m, 1H), 7.89 (d, J = 3.4 Hz, 1H), 7.89–7.86 (m, 1H), 7.78 (dd, J = 8.4, 1.7 Hz, 1H), 7.64 (dd, J = 7.5, 1.7 Hz, 1H), 7.54 (d, J = 8.2 Hz, 1H), 7.38–7.33 (m, 2H), 7.21–7.16 (m, 1H), 7.07 (td, J = 7.5, 0.9 Hz, 1H), 3.91 (s, 3H); ^{13}C NMR (101 MHz, DMSO- d_6) δ 173.2, 165.4, 164.4, 161.9, 157.0, 155.4, 145.8, 144.7, 139.9, 139.8, 135.1, 132.6, 132.3, 130.1, 130.0, 129.9, 129.3, 126.1, 125.5, 123.8, 122.0, 121.0, 120.7, 119.7, 116.7, 116.5, 116.3, 112.5, 56.4; HR-ESI-MS calcd for $\text{C}_{29}\text{H}_{20}\text{FNO}_5$ $[\text{M} + \text{H}]^+$ 482.1326; found 488.1379.

4.6.8 *N*-(3-(7-(4-Fluorophenyl)-3-hydroxy-4-oxo-4*H*-chromen-2-yl)phenyl)-2-methylbenzamide (7h). Light yellow solid. Yield 61%. Mp 235.3–237.1 °C. ^1H NMR (400 MHz, DMSO- d_6) δ 10.58 (s, 1H), 9.68 (s, 1H), 8.63 (s, 1H), 8.16 (d, J = 8.4 Hz, 1H), 7.98 (d, J = 1.7 Hz, 1H), 7.97–7.94 (m, 1H), 7.92 (d, J = 5.9 Hz, 1H), 7.91 (d, J = 3.2 Hz, 1H), 7.90–7.87 (m, 1H), 7.78 (dd, J = 8.4, 1.7 Hz, 1H), 7.56–7.48 (m, 2H), 7.42–7.37 (m, 1H), 7.36 (d, J = 7.0 Hz, 1H), 7.35–7.33 (m, 1H), 7.31 (d, J = 7.4 Hz, 2H), 2.40 (s, 3H); ^{13}C NMR (101 MHz, DMSO- d_6) δ 173.2, 168.6, 161.9, 155.5, 145.8, 144.7, 140.0, 139.9, 137.6, 135.8, 135.1, 132.2, 131.1, 130.2, 130.0, 129.9, 129.4, 127.8, 126.2, 126.1, 123.8, 123.6, 121.8, 120.7, 119.6, 116.7, 116.5, 116.2, 19.9; HR-ESI-MS calcd for $\text{C}_{29}\text{H}_{20}\text{FNO}_4$ $[\text{M} + \text{H}]^+$ 466.1376; found 466.1435.

4.6.9 *N*-(3-(7-(4-Fluorophenyl)-3-hydroxy-4-oxo-4*H*-chromen-2-yl)phenyl)-4-(trifluoromethyl)benzamide (7i). Light yellow solid. Yield 67%. Mp 272.3–273.2 °C. ^1H NMR (400 MHz, DMSO- d_6) δ 10.87 (s, 1H), 9.73 (s, 1H), 8.70 (s, 1H), 8.25 (d, J = 8.2 Hz, 2H), 8.17 (d, J = 8.4 Hz, 1H), 8.02 (dd, J = 7.7,

1.2 Hz, 2H), 8.00–7.96 (m, 1H), 7.94 (d, J = 7.2 Hz, 1H), 7.92 (s, 1H), 7.91 (s, 1H), 7.90–7.87 (m, 1H), 7.78 (dd, J = 8.4, 1.7 Hz, 1H), 7.56 (t, J = 8.0 Hz, 1H), 7.41–7.32 (m, 2H); ^{13}C NMR (101 MHz, DMSO- d_6) δ 173.2, 165.1, 161.9, 155.5, 145.7, 144.7, 139.9, 139.5, 135.1, 135.1, 132.2, 130.0, 129.3, 126.1, 125.9, 125.9, 125.8, 124.0, 123.7, 123.1, 122.8, 120.7, 120.5, 116.7, 116.5, 116.2, 31.2; HR-ESI-MS calcd for $\text{C}_{29}\text{H}_{17}\text{F}_4\text{NO}_4$ $[\text{M} + \text{H}]^+$ 520.1094; found 520.1152.

4.6.10 4-Bromo-*N*-(3-(7-(4-fluorophenyl)-3-hydroxy-4-oxo-4*H*-chromen-2-yl)phenyl)benzamide (7j). Light yellow solid. Yield 69%. Mp 268.2–268.9 °C. ^1H NMR (400 MHz, DMSO- d_6) δ 10.55 (d, J = 8.9 Hz, 1H), 9.73 (s, 1H), 8.62 (s, 1H), 8.17 (d, J = 8.4 Hz, 1H), 8.04–7.98 (m, 2H), 7.98–7.95 (m, 2H), 7.95–7.93 (m, 1H), 7.92 (d, J = 3.2 Hz, 1H), 7.90 (d, J = 5.3 Hz, 1H), 7.81–7.78 (m, 1H), 7.78 (s, 1H), 7.77 (d, J = 1.9 Hz, 1H), 7.56 (t, J = 8.0 Hz, 1H), 7.36 (t, J = 8.8 Hz, 2H); ^{13}C NMR (101 MHz, DMSO- d_6) δ 173.2, 165.2, 162.0, 155.5, 145.7, 144.7, 139.9, 139.6, 135.2, 134.3, 132.2, 132.0, 130.4, 130.0, 129.9, 129.3, 126.1, 126.0, 123.9, 123.7, 122.7, 120.7, 120.5, 116.7, 116.5, 116.2; HR-ESI-MS calcd for $\text{C}_{28}\text{H}_{17}\text{BrFNO}_4$ $[\text{M} + \text{H}]^+$ 530.0325; found 530.0381. $[\text{M} + 2 + \text{H}]^+$ 532.0325; found 532.0359.

4.6.11 *N*-(3-(7-(4-Fluorophenyl)-3-hydroxy-4-oxo-4*H*-chromen-2-yl)phenyl)-3-methoxybenzamide (7k). Light yellow solid. Yield 71%. Mp 243.6–244.7 °C. ^1H NMR (400 MHz, DMSO- d_6) δ 10.60 (s, 1H), 9.70 (s, 1H), 8.70 (t, J = 1.9 Hz, 1H), 8.18 (d, J = 8.4 Hz, 1H), 8.03 (d, J = 1.6 Hz, 1H), 8.01 (ddd, J = 8.0, 1.7, 1.0 Hz, 1H), 7.97 (ddd, J = 8.2, 2.1, 1.0 Hz, 1H), 7.94–7.90 (m, 2H), 7.79 (dd, J = 8.4, 1.7 Hz, 1H), 7.64 (ddd, J = 7.7, 1.5, 0.9 Hz, 1H), 7.60 (dd, J = 2.5, 1.6 Hz, 1H), 7.56 (t, J = 8.0 Hz, 1H), 7.46 (t, J = 7.9 Hz, 1H), 7.39–7.34 (m, 2H), 7.18 (ddd, J = 8.2, 2.6, 0.9 Hz, 1H), 3.87 (s, 3H); ^{13}C NMR (101 MHz, DMSO- d_6) δ 173.2, 165.9, 162.0, 159.7, 155.5, 145.8, 144.7, 139.9, 139.8, 136.6, 135.2, 135.1, 132.2, 130.1, 130.0, 129.9, 126.1, 123.8, 123.8, 122.9, 120.7, 120.6, 118.1, 116.7, 116.5, 116.3, 113.5, 55.9; HR-ESI-MS calcd for $\text{C}_{29}\text{H}_{20}\text{FNO}_5$ $[\text{M} + \text{H}]^+$ 482.1326; found 482.1385.

4.6.12 *N*-(3-(7-(4-Fluorophenyl)-3-hydroxy-4-oxo-4*H*-chromen-2-yl)phenyl)-3-methylbenzamide (7l). Yellow solid. Yield 63%. Mp 239.5–240.4 °C. ^1H NMR (400 MHz, DMSO- d_6) δ 10.48 (s, 1H), 9.67 (s, 1H), 8.62 (t, J = 1.9 Hz, 1H), 8.13 (d, J = 8.4 Hz, 1H), 8.02 (s, 1H), 8.01–8.00 (m, 1H), 7.98 (s, 1H), 7.95 (dt, J = 7.9, 1.0 Hz, 1H), 7.91 (dd, J = 7.4, 2.0 Hz, 1H), 7.88 (dd, J = 8.8, 5.4 Hz, 2H), 7.81 (s, 1H), 7.75 (dd, J = 8.4, 1.7 Hz, 1H), 7.51 (t, J = 8.0 Hz, 1H), 7.37 (d, J = 1.0 Hz, 1H), 7.32 (t, J = 8.8 Hz, 2H), 2.37 (s, 3H); ^{13}C NMR (101 MHz, DMSO- d_6) δ 173.25, 166.34, 161.95, 155.49, 146.15, 145.82, 144.73, 142.71, 139.91, 138.22, 135.22, 135.13, 132.78, 132.17, 130.02, 129.94, 129.25, 128.82, 128.79, 127.63, 126.12, 125.48, 123.74, 120.71, 120.44, 116.70, 116.49, 116.27, 21.51; HR-ESI-MS calcd for $\text{C}_{29}\text{H}_{20}\text{FNO}_4$ $[\text{M} + \text{H}]^+$ 466.1376; found 466.1435.

4.6.13 3-Fluoro-*N*-(3-(7-(4-fluorophenyl)-3-hydroxy-4-oxo-4*H*-chromen-2-yl)phenyl)benzamide (7m). Light yellow solid. Yield 64%. Mp 242.2–243.5 °C. ^1H NMR (400 MHz, DMSO- d_6) δ 10.60 (s, 1H), 9.72 (s, 1H), 8.65 (t, J = 1.7 Hz, 1H), 8.18 (d, J = 8.4 Hz, 1H), 8.05–8.00 (m, 2H), 7.97–7.94 (m, 1H), 7.93 (d, J

= 5.5 Hz, 1H), 7.91 (s, 1H), 7.89 (d, $J = 7.5$ Hz, 1H), 7.87–7.83 (m, 1H), 7.79 (dd, $J = 8.4, 1.3$ Hz, 1H), 7.65–7.59 (m, 1H), 7.57 (t, $J = 7.8$ Hz, 1H), 7.51–7.44 (m, 1H), 7.37 (t, $J = 8.8$ Hz, 2H); ^{13}C NMR (101 MHz, DMSO- d_6) δ 173.2, 162.4, 155.5, 146.2, 145.7, 144.7, 142.7, 139.9, 139.6, 137.5, 135.2, 132.2, 131.1, 130.0, 129.9, 129.3, 127.6, 127.6, 126.1, 124.6, 124.0, 122.8, 120.7, 120.6, 116.7, 116.5, 115.3, 115.1; HR-ESI-MS calcd for $\text{C}_{28}\text{H}_{17}\text{F}_2\text{NO}_4$ $[\text{M} + \text{H}]^+$ 470.1126; found 470.1185.

4.6.14 4-Ethyl-N-(3-(7-(4-fluorophenyl)-3-hydroxy-4-oxo-4H-chromen-2-yl)phenyl)benzamide (7n). Light yellow solid. Yield 73%. Mp 257.6–258.5 °C. ^1H NMR (400 MHz, DMSO- d_6) δ 10.46 (s, 1H), 9.69 (s, 1H), 8.66 (t, $J = 1.9$ Hz, 1H), 8.17 (d, $J = 8.4$ Hz, 1H), 8.00 (d, $J = 1.6$ Hz, 1H), 8.00–7.97 (m, 1H), 7.97 (s, 1H), 7.97–7.95 (m, 1H), 7.94 (dt, $J = 2.2, 1.0$ Hz, 1H), 7.93–7.88 (m, 2H), 7.78 (dd, $J = 8.4, 1.6$ Hz, 1H), 7.54 (t, $J = 8.0$ Hz, 1H), 7.38 (s, 1H), 7.37 (s, 1H), 7.36 (d, $J = 3.3$ Hz, 1H), 7.33 (d, $J = 2.0$ Hz, 1H), 2.69 (q, $J = 7.6$ Hz, 2H), 1.21 (t, $J = 7.6$ Hz, 3H); ^{13}C NMR (101 MHz, DMSO- d_6) δ 173.2, 166.1, 161.9, 155.5, 148.4, 145.8, 144.7, 140.0, 139.9, 135.2, 135.1, 132.7, 132.2, 130.0, 129.9, 129.2, 128.4, 128.3, 126.1, 123.7, 122.7, 120.7, 120.4, 116.7, 116.5, 116.2, 28.6, 15.9; HR-ESI-MS calcd for $\text{C}_{30}\text{H}_{22}\text{FNO}_4$ $[\text{M} + \text{H}]^+$ 480.1533; found 480.1595.

4.6.15 4-Bromo-2-fluoro-N-(3-(7-(4-fluorophenyl)-3-hydroxy-4-oxo-4H-chromen-2-yl)phenyl)benzamide (7o). Yellow solid. Yield 61%. Mp 243.8–244.2 °C. ^1H NMR (400 MHz, DMSO- d_6) δ 10.77 (s, 1H), 9.72 (s, 1H), 8.61–8.46 (m, 1H), 8.16 (dd, $J = 8.4, 2.5$ Hz, 1H), 8.02–7.99 (m, 1H), 7.99–7.97 (m, 1H), 7.93–7.91 (m, 1H), 7.90 (d, $J = 2.2$ Hz, 1H), 7.89 (d, $J = 2.2$ Hz, 1H), 7.80–7.73 (m, 2H), 7.70–7.65 (m, 1H), 7.58 (d, $J = 1.9$ Hz, 1H), 7.57–7.56 (m, 1H), 7.38–7.33 (m, 2H); ^{13}C NMR (101 MHz, DMSO- d_6) δ 173.2, 171.0, 162.7, 162.0, 145.6, 144.8, 140.0, 139.4, 135.1, 132.4, 132.1, 130.1, 130.0, 129.9, 129.5, 128.3, 126.1, 124.8, 123.9, 123.8, 121.9, 120.7, 120.2, 120.0, 119.8, 116.7, 116.5, 116.2; HR-ESI-MS calcd for $\text{C}_{28}\text{H}_{16}\text{BrF}_2\text{NO}_4$ $[\text{M} + \text{H}]^+$ 548.0231; found 548.0297; $[\text{M} + 2 + \text{H}]^+$ 550.0244; found 550.0275.

4.6.16 4-fluoro-N-(3-(7-(4-fluorophenyl)-3-hydroxy-4-oxo-4H-chromen-2-yl)phenyl)-3-meth-yl benzamide (7p). Light yellow solid. Yield 66%. Mp 219.9–221.4 °C. ^1H NMR (400 MHz, DMSO- d_6) δ 10.47 (s, 1H), 9.70 (s, 1H), 8.61 (s, 1H), 8.16 (dd, $J = 8.3, 4.9$ Hz, 1H), 8.00 (s, 1H), 7.96 (d, $J = 1.9$ Hz, 1H), 7.92 (s, 1H), 7.91 (s, 1H), 7.89 (s, 1H), 7.89 (s, 1H), 7.78 (d, $J = 7.5$ Hz, 1H), 7.55 (t, $J = 8.0$ Hz, 1H), 7.36 (t, $J = 8.7$ Hz, 2H), 7.33–7.27 (m, 1H), 2.32 (d, $J = 1.5$ Hz, 3H); ^{13}C NMR (101 MHz, CDCl_3) δ 178.0, 171.8, 170.0, 166.7, 160.2, 158.7, 150.5, 149.5, 144.8, 144.7, 144.6, 139.9, 137.0, 136.12136.1, 134.8, 134.7, 134.0, 129.8, 129.6, 128.5, 125.5, 121.5, 121.2, 120.4, 120.2, 19.5; HR-ESI-MS calcd for $\text{C}_{29}\text{H}_{19}\text{F}_2\text{NO}_4$ $[\text{M} + \text{H}]^+$ 484.1282; found 484.1350.

4.6.17 2-Fluoro-N-(3-(7-(4-fluorophenyl)-3-hydroxy-4-oxo-4H-chromen-2-yl)phenyl)-4-meth-oxybenzamide (7q). Light yellow solid. Yield 67%. Mp 235.2–237.0 °C. ^1H NMR (400 MHz, DMSO- d_6) δ 10.43 (s, 1H), 9.69 (s, 1H), 8.58 (t, $J = 1.8$ Hz, 1H), 8.16 (dd, $J = 8.4, 1.8$ Hz, 1H), 7.98 (d, $J = 1.8$ Hz, 1H), 7.98–7.94 (m, 1H), 7.93–7.90 (m, 1H), 7.89 (d, $J = 1.6$ Hz, 1H), 7.88 (d, $J = 2.2$ Hz, 1H), 7.77 (dd, $J = 8.4, 1.7$ Hz, 1H), 7.68 (t, $J = 8.6$ Hz, 1H), 7.53 (t, $J = 8.0$ Hz, 1H), 7.37–7.32 (m, 2H), 6.96

(dd, $J = 12.5, 2.4$ Hz, 1H), 6.90 (dd, $J = 8.6, 2.5$ Hz, 1H), 3.84 (s, 3H); ^{13}C NMR (101 MHz, DMSO- d_6) δ 173.2, 163.2, 162.5, 160.9, 155.5, 145.7, 144.7, 139.9, 139.7, 135.2, 132.3, 131.8, 131.8, 130.0, 129.9, 129.4, 126.1, 123.7, 120.7, 119.8, 117.2, 117.1, 116.7, 116.5, 116.2, 111.1, 102.5, 102.3, 56.5; HR-ESI-MS calcd for $\text{C}_{29}\text{H}_{19}\text{F}_2\text{NO}_5$ $[\text{M} + \text{H}]^+$ 500.1231; found 500.1302.

4.6.18 N-(3-(7-(4-Fluorophenyl)-3-hydroxy-4-oxo-4H-chromen-2-yl)phenyl)-3,5-dimethoxy-benzamide (7r). Light yellow solid. Yield 72%. Mp 222.1–224.0 °C. ^1H NMR (400 MHz, DMSO- d_6) δ 10.49 (s, 1H), 9.69 (s, 1H), 8.67–8.63 (m, 1H), 8.16 (dd, $J = 8.4, 3.9$ Hz, 1H), 8.01 (d, $J = 1.6$ Hz, 1H), 8.00–7.97 (m, 1H), 7.92 (d, $J = 3.5$ Hz, 1H), 7.91 (s, 1H), 7.90–7.88 (m, 1H), 7.78 (dd, $J = 8.4, 1.7$ Hz, 1H), 7.54 (t, $J = 8.0$ Hz, 1H), 7.38–7.32 (m, 2H), 7.18 (d, $J = 2.3$ Hz, 2H), 6.71 (t, $J = 2.2$ Hz, 1H), 3.82 (s, 6H); ^{13}C NMR (101 MHz, CDCl_3) δ 178.0, 170.5, 166.7, 165.7, 160.2, 150.6, 149.5, 144.6, 144.5, 142.0, 139.9, 136.9, 134.8, 134.7, 134.0, 130.9, 128.7, 128.6, 127.7, 125.5, 121.4, 121.2, 121.0, 111.0, 108.8, 60.8; HR-ESI-MS calcd for $\text{C}_{30}\text{H}_{22}\text{FNO}_6$ $[\text{M} + \text{H}]^+$ 512.1431; found 512.1502.

4.6.19 N-(3-(7-(4-Fluorophenyl)-3-hydroxy-4-oxo-4H-chromen-2-yl)phenyl)-3,5-dimethylbenzamide (7s). Light yellow solid. Yield 69%. Mp 272.3–273.6 °C. ^1H NMR (400 MHz, DMSO- d_6) δ 10.44 (s, 1H), 9.69 (s, 1H), 8.64 (t, $J = 1.8$ Hz, 1H), 8.17 (d, $J = 8.4$ Hz, 1H), 8.01 (d, $J = 1.5$ Hz, 1H), 8.00–7.93 (m, 2H), 7.93–7.90 (m, 1H), 7.89 (dd, $J = 5.2, 3.0$ Hz, 1H), 7.78 (dd, $J = 8.4, 1.6$ Hz, 1H), 7.63 (s, 2H), 7.54 (t, $J = 8.0$ Hz, 1H), 7.36 (t, $J = 8.8$ Hz, 2H), 7.22 (s, 1H), 2.36 (s, 6H); ^{13}C NMR (101 MHz, DMSO- d_6) δ 173.20, 166.41, 161.90, 155.43, 145.79, 144.69, 139.89, 139.83, 138.03, 138.03, 135.19, 135.12, 135.08, 133.42, 132.11, 129.96, 129.87, 129.18, 126.06, 125.94, 125.94, 123.72, 122.61, 120.65, 120.33, 116.64, 116.42, 116.17, 21.35, 21.35; HR-ESI-MS calcd for $\text{C}_{30}\text{H}_{24}\text{FNO}_4$ $[\text{M} + \text{H}]^+$ 480.1533; found 480.1604.

4.6.20 6-Chloro-N-(3-(7-(4-fluorophenyl)-3-hydroxy-4-oxo-4H-chromen-2-yl)phenyl)nicotinamide (7t). Yellow solid. Yield 75%. Mp 248.5–249.9 °C. ^1H NMR (400 MHz, DMSO- d_6) δ 10.88 (s, 1H), 9.73 (s, 1H), 9.03 (d, $J = 2.3$ Hz, 1H), 8.67 (s, 1H), 8.46 (dd, $J = 8.3, 2.5$ Hz, 1H), 8.17 (d, $J = 8.3$ Hz, 1H), 8.03 (s, 1H), 8.01 (s, 1H), 7.96 (d, $J = 8.2$ Hz, 1H), 7.91 (dd, $J = 8.4, 5.4$ Hz, 2H), 7.78 (d, $J = 8.1$ Hz, 1H), 7.72 (d, $J = 8.3$ Hz, 1H), 7.57 (t, $J = 8.0$ Hz, 1H), 7.36 (t, $J = 8.7$ Hz, 2H); ^{13}C NMR (101 MHz, DMSO- d_6) δ 173.2, 163.6, 161.9, 155.4, 153.3, 150.0, 145.5, 144.7, 139.9, 139.7, 139.3, 135.1, 132.2, 130.2, 129.9, 129.8, 129.3, 126.0, 124.6, 124.0, 123.7, 122.6, 120.6, 120.4, 116.6, 116.4, 116.2; HR-ESI-MS calcd for $\text{C}_{27}\text{H}_{16}\text{ClFN}_2\text{O}_4$ $[\text{M} + \text{H}]^+$ 487.0783; found 487.0853.

4.6.21 3,5-Difluoro-N-(3-(7-(4-fluorophenyl)-3-hydroxy-4-oxo-4H-chromen-2-yl)phenyl)benzamide (7u). Light yellow solid. Yield 73%. Mp 246.4–247.9 °C. ^1H NMR (400 MHz, DMSO- d_6) δ 10.72 (s, 1H), 9.71 (s, 1H), 8.65 (t, $J = 1.6$ Hz, 1H), 8.15 (d, $J = 8.4$ Hz, 1H), 8.02 (s, 1H), 8.00 (s, 1H), 7.96–7.92 (m, 1H), 7.90 (dd, $J = 8.6, 5.4$ Hz, 2H), 7.79 (d, $J = 2.0$ Hz, 1H), 7.77 (s, 1H), 7.76 (s, 1H), 7.58–7.54 (m, 1H), 7.51 (dt, $J = 9.1, 2.3$ Hz, 1H), 7.35 (t, $J = 8.8$ Hz, 2H); ^{13}C NMR (101 MHz, DMSO- d_6) δ 173.2, 164.0, 163.5, 161.5, 155.4, 145.6, 144.7,

139.9, 139.3, 138.6, 135.1, 132.2, 130.0, 129.9, 129.3, 127.1, 126.0, 124.1, 123.7, 122.8, 120.6, 120.6, 116.6, 116.4, 116.2, 111.9, 111.6. HR-ESI-MS calcd for $C_{28}H_{16}F_3NO_4$ $[M + H]^+$ 488.1031; found 488.1104.

4.6.22 2,4-Dichloro-*N*-(3-(7-(4-fluorophenyl)-3-hydroxy-4-oxo-4H-chromen-2-yl)phenyl)pyrimidine-5-carboxamide (7v). Light yellow solid. Yield 72%. Mp 243.8–245.7 °C. 1H NMR (400 MHz, DMSO- d_6) δ 11.18 (s, 1H), 9.79 (s, 1H), 9.13 (s, 1H), 8.56 (t, $J = 1.8$ Hz, 1H), 8.16 (d, $J = 8.4$ Hz, 1H), 8.02 (d, $J = 8.0$ Hz, 1H), 7.99 (d, $J = 1.5$ Hz, 1H), 7.94–7.92 (m, 1H), 7.91–7.90 (m, 1H), 7.90–7.87 (m, 1H), 7.78 (dd, $J = 8.4, 1.6$ Hz, 1H), 7.60 (t, $J = 8.1$ Hz, 1H), 7.36 (t, $J = 8.8$ Hz, 2H); ^{13}C NMR (101 MHz, DMSO- d_6) δ 173.2, 163.6, 161.9, 155.4, 153.3, 150.0, 145.5, 144.7, 139.9, 139.7, 139.3, 135.1, 132.2, 130.2, 129.9, 129.8, 129.3, 126.0, 124.6, 123.7, 122.7, 120.6, 120.4, 116.6, 116.4, 116.2. HR-ESI-MS calcd for $C_{26}H_{14}Cl_2FN_3O_4$ $[M + H]^+$ 522.3134; found 522.4187.

4.6.23 4-Cyano-*N*-(3-(7-(4-fluorophenyl)-3-hydroxy-4-oxo-4H-chromen-2-yl)phenyl)benzamide (7w). Yellow solid. Yield 69%. Mp 261.6–262.9 °C. 1H NMR (400 MHz, DMSO- d_6) δ 10.88 (s, 1H), 9.71 (s, 1H), 8.68 (s, 1H), 8.20 (d, $J = 8.3$ Hz, 2H), 8.16 (d, $J = 8.4$ Hz, 1H), 8.04 (s, 1H), 8.02 (s, 1H), 7.97 (q, $J = 2.4, 1.6$ Hz, 2H), 7.91 (dd, $J = 8.7, 5.4$ Hz, 2H), 7.79 (dd, $J = 8.4, 1.4$ Hz, 1H), 7.56 (t, $J = 8.0$ Hz, 1H), 7.36 (t, $J = 8.8$ Hz, 2H); ^{13}C NMR (101 MHz, DMSO- d_6) δ 173.2, 164.8, 155.4, 145.6, 144.7, 143.6, 139.9, 139.5, 139.2, 136.9, 133.2, 132.9, 132.2, 130.4, 130.1, 129.9, 129.8, 129.6, 129.3, 129.2, 128.2, 126.1, 120.7, 120.6, 116.7, 116.5, 114.4; HR-ESI-MS calcd for $C_{29}H_{17}FN_2O_4$ $[M + H]^+$ 477.1172; found 477.3286.

4.6.24 *N*-(3-(7-(4-Fluorophenyl)-3-hydroxy-4-oxo-4H-chromen-2-yl)phenyl)-4-nitrobenzamide (7x). Light yellow solid. Yield 70%. Mp 262.3–263.4 °C. 1H NMR (400 MHz, DMSO- d_6) δ 10.96 (s, 1H), 9.71 (s, 1H), 8.68 (t, $J = 1.7$ Hz, 1H), 8.36 (d, $J = 8.9$ Hz, 2H), 8.28 (d, $J = 8.9$ Hz, 2H), 8.16 (d, $J = 8.4$ Hz, 1H), 8.02 (d, $J = 9.1$ Hz, 2H), 8.00–7.95 (m, 1H), 7.90 (dd, $J = 8.8, 5.4$ Hz, 2H), 7.77 (dd, $J = 8.4, 1.5$ Hz, 1H), 7.56 (t, $J = 8.0$ Hz, 1H), 7.35 (t, $J = 8.8$ Hz, 2H); ^{13}C NMR (101 MHz, DMSO- d_6) δ 173.2, 164.51, 161.90, 155.42, 149.67, 145.57, 144.67, 140.80, 139.90, 139.40, 135.11, 132.21, 129.94, 129.90, 129.90, 129.85, 129.28, 126.04, 124.12, 123.97, 123.97, 123.69, 122.75, 120.64, 120.54, 116.63, 116.42, 116.21; HR-ESI-MS calcd for $C_{28}H_{17}FN_2O_6$ $[M + H]^+$ 497.1076; found 497.1976.

4.6.25 *N*-(3-(7-(4-Fluorophenyl)-3-hydroxy-4-oxo-4H-chromen-2-yl)phenyl)-[1,1'-biphenyl]-4-carboxamide (7y). Yellow solid. Yield 63%. Mp 254.8–256.1 °C. 1H NMR (400 MHz, DMSO- d_6) δ 10.65 (s, 1H), 9.71 (s, 1H), 8.72 (t, $J = 1.7$ Hz, 1H), 8.19 (d, $J = 8.5$ Hz, 1H), 8.18 (s, 1H), 8.15 (s, 1H), 8.04 (d, $J = 1.4$ Hz, 1H), 8.01 (dt, $J = 8.2, 2.1$ Hz, 2H), 7.96–7.91 (m, 2H), 7.86 (d, $J = 8.4$ Hz, 2H), 7.83–7.78 (m, 2H), 7.77 (s, 1H), 7.57 (t, $J = 8.0$ Hz, 1H), 7.52 (t, $J = 7.6$ Hz, 2H), 7.44 (dd, $J = 8.3, 6.3$ Hz, 1H), 7.38 (t, $J = 8.8$ Hz, 2H); ^{13}C NMR (101 MHz, DMSO- d_6) δ 173.2, 165.8, 161.9, 155.5, 145.8, 144.7, 143.7, 139.9, 139.8, 139.6, 135.1, 135.1, 133.9, 132.1, 130.0, 129.9, 129.6, 129.2, 129.0, 128.7, 127.4, 127.0, 126.1, 123.8, 122.7, 120.7, 120.4, 116.7, 116.4, 116.2; HR-ESI-MS calcd for $C_{34}H_{22}FNO_4$ $[M + H]^+$ 528.1533; found 528.1605.

4.6.26 *N*-(3-(7-(4-Fluorophenyl)-3-hydroxy-4-oxo-4H-chromen-2-yl)phenyl)-4-propylbenzamide (7z). Light yellow solid. Yield 64%. Mp 245.3–246.4 °C. 1H NMR (400 MHz, DMSO- d_6) δ 10.52 (s, 1H), 9.69 (s, 1H), 8.69 (t, $J = 1.9$ Hz, 1H), 8.18 (d, $J = 8.4$ Hz, 1H), 8.03 (d, $J = 1.6$ Hz, 1H), 8.01–7.98 (m, 2H), 7.98–7.95 (m, 2H), 7.95–7.90 (m, 2H), 7.80 (dd, $J = 8.4, 1.7$ Hz, 1H), 7.55 (t, $J = 8.0$ Hz, 1H), 7.39 (d, $J = 2.1$ Hz, 1H), 7.37 (d, $J = 1.9$ Hz, 1H), 7.36 (s, 1H), 7.35 (d, $J = 1.3$ Hz, 1H), 2.68–2.61 (m, 2H), 1.64 (h, $J = 7.3$ Hz, 2H), 0.91 (t, $J = 7.3$ Hz, 3H); ^{13}C NMR (101 MHz, DMSO- d_6) δ 173.2, 166.1, 161.9, 155.4, 146.7, 145.8, 144.7, 140.0, 139.8, 135.1, 132.6, 132.1, 130.0, 129.9, 129.2, 128.8, 128.35, 126.1, 123.7, 122.7, 120.7, 120.1, 116.6, 116.4, 116.2, 37.5, 24.37, 14.1; HR-ESI-MS calcd for $C_{31}H_{24}FNO_4$ $[M + H]^+$ 494.1689; found 494.1760.

4.7 *In vitro* cytotoxicity against seven different cancer cell lines

The human cancer cell lines HCC1937, A549, HeLa, and GTL-16 were cultured in RPMI medium 1640 with 10% FBS, 100 U mL⁻¹ penicillin, and 100 mg mL⁻¹ streptomycin, whereas MDA-MB-231, MCF-7, and Hep G2 were cultured in high sugar DMEM medium with 10% FBS, 100 U mL⁻¹ penicillin, and 100 mg mL⁻¹ streptomycin. All the cells were incubated in an incubator at 37 °C with 5% CO₂, and all the experiments were performed while the cells were in the logarithmic growth phase. Cells were inoculated in 96-well plates at a density of 4×10^3 – 6×10^3 cells per well and incubated for 24 h. After the cells were fully plastered, 100 μ L of serum-free medium with various concentrations of compounds was added and incubated at 37 °C for 72 h. A cell viability assay (CCK8 assay) was performed after compound administration. LY294002 and 5-fluorouracil were selected as positive controls, and both blank and zeroed groups were set up. A 10% CCK8 solution was added to each well in a final volume of 110 μ L and incubated at 37 °C for 2 h. The absorbance (optical density, OD) at 450 nm and 630 nm was measured on a multifunctional microplate analyzer (Mithras2 LB943, Berthold, Germany). The concentration of a compound that inhibited cell growth by 50% (IC₅₀) was processed by SPSS 19.0 statistical software. The inhibition rate was calculated by the formula $[1 - (\text{experimental group} - \text{background group}) / (\text{blank group} - \text{zero-adjusted group})] \times 100\%$. Five replicate wells were set up for each experimental group, and the results of three independent experiments were expressed as mean \pm SD.

4.8 Colony-formation assay

The MDA-MB-231 cells were inoculated at 800 cells per well in 12-well plates with 3 replicate wells per group and incubated in an incubator at 37 °C with 5% CO₂ for 5–7 days. When 30–50 cell clusters were formed, the drug was added and incubation was continued for 24 h, 48 h, and 72 h. The old medium was removed, the cells were washed twice with pre-cooled PBS, and fixed with 4% paraformaldehyde for 30 minutes. The fixative was removed, and a 0.5% crystal violet

staining solution was added. The cells were then gently washed with water and air-dried. The clones were photographed using a gel imager and counted by ImageJ software.

4.9 Hoechst staining assay

The MDA-MB-231 cells were inoculated in 6-well plates at 2×10^5 – 3×10^5 per well and incubated overnight in an incubator at 37 °C with 5% CO₂. After the cells were plated, the drug was added and incubated for 48 h. The old solution was removed, the cells were washed twice with PBS, and methanol was added to fix the cells for 30 minutes. The cells were washed twice with PBS to remove the methanol, 500 μL of Hoechst 33258 staining solution was added to each well and the cells were stained for 30 minutes at room temperature with protection from light. Cells were assessed morphologically using a fluorescence microscope.

4.10 Cell cycle assay

The MDA-MB-231 cells were treated with different concentrations of compound **7t** for 48 h, digested with trypsin, and collected from the walled cells. After centrifugation, the supernatant was discarded, the cells were washed 2–3 times with PBS, and collected so that each sample contained approximately 1×10^6 cells per mL. 500 μL of pre-cooled 70% ethanol was added and fixed overnight at 4 °C. A centrifuge was used to remove the ethanol, the cells were resuspended with PBS, and the cell suspension was filtered through a 200-mesh nylon membrane. A CytoFLEX flow cytometer (Beckman Coulter, USA) was used to measure the cell cycle, and the excitation wavelength of red fluorescence was measured at 488 nm.

4.11 Annexin V-FITC/PI double staining assay for detection of apoptosis

The MDA-MB-231 cells were treated with different concentrations of compound **7t** for 48 h, digested with trypsin, and collected from the walled cells. After centrifugation, the supernatant was discarded, the cells were washed 2–3 times with PBS, and collected so that each sample contained approximately 5×10^5 cells per mL. The cells were resuspended with 500 μL of binding buffer, 5 μL of Annexin V-FITC and 5 μL of PI were added, and the reaction was carried out at room temperature and protected from light for 15 minutes. Then the cells were detected by a CytoFLEX flow cytometer (Beckman Coulter, USA) with an excitation wavelength of Ex = 488 nm and an emission wavelength of Em = 530 nm.

4.12 Wound healing migration assay

The MDA-MB-231 cells were inoculated and cultured in 6-well plates at 4×10^5 cells per well overnight. After the cells were adhered to the wall, they were scribed with a sterilized 200 μL gun tip, washed with PBS solution to remove the scribed

cells, and incubated with the normal medium or compound **7t**. Photographs were taken with a phase contrast microscope at time points of 0, 12 h, 24 h, and 48 h of incubation.

4.13 Transwell invasion assays

The MDA-MB-231 cells in the logarithmic growth phase were counted by trypsin digestion with a counting plate, and single cell suspensions were prepared by resuspension in serum-free medium at a density of 5×10^5 cells per well. A total of 600 μL of complete medium was added to the lower chamber of the Transwell chamber. A cell suspension of 200 μL per well was uniformly added dropwise to the upper chamber, along with different concentrations of compound **7t**, and placed in an incubator at 37 °C for 48 h. The upper chamber medium was removed and allowed to soak in methanol for 2 h for fixation. Non-invasive cells in the upper chamber were removed with a sterile swab containing PBS, then inverted and air-dried. Cells in the small chamber were stained with 500 μL of 0.5% crystalline violet for 30 minutes, then washed with PBS and air-dried, photographed with a microscope, and counted using ImageJ software.

4.14 Western blotting analysis

The MDA-MB-231 cells were incubated in 6-well plates with different concentrations of compound **7t** at 37 °C for 12 h, trypsin digested, washed with PBS, and centrifuged to obtain cell samples. A protein lysis solution (10× RIPA + 1× PMSF) was added at 0 °C and the cells were fully lysed for 30 min. The samples were placed at 14 000 × g and centrifuged at 4 °C for 10 minutes, and the supernatant was the extracted protein. The protein concentration was determined using the BCA protein assay kit. Protein samples (40 μg) were processed by SDS-PAGE gel electrophoresis and then transferred to PVDF membranes. The PVDF membrane strips containing the target proteins were blocked with 5% skim milk powder and then incubated with the primary antibody at 4 °C overnight. The membrane strips were removed and washed three times with TBST. The strips are incubated with the secondary antibody for 2 h at room temperature. The strips were removed and washed three times with TBST for five minutes each time. The developing solution (1:1 ratio of liquid A to liquid B, which can be used directly) was evenly dropped onto the protein side of the strips and incubated for one minute at room temperature. After incubation, the strips were transferred to a gel imager for exposure imaging.

4.15 Molecular modeling

Surflex-dock in Sybyl 2.1 was used for molecular docking. The structures of small molecules were built in the Sybyl package with standard bond lengths and angles and minimized using the Powell method. The termination of the gradient, force field of Tripos and charge of Gasteiger–Hückel were applied for the minimization process. The AMBER FF99 force field was applied for the protein after extracting all the non-polar water and addition of hydrogen atoms. The

standard docking procedures were performed with parameters set in default. The reliability of the docking strategy was verified by re-docking the original ligand into the crystal structure. After docking, residues within 5 Å of the inhibitors were identified and the conformations that appeared the most frequently and possessed the lowest binding free energy were selected for further analysis. Binding modes and interactions were analyzed in Pymol.

Conflicts of interest

The authors declare that they have no known competing financial interests or personal relationships that could have appeared to influence the work reported in this paper.

Acknowledgements

We gratefully acknowledge the financial support from High-level University Construction Fund of Guangdong Province (grant number: 06-410-2107203, 06-410-2107252, 06-410-2107284); Medical Scientific Research Foundation of Guangdong Province of China (grant number: A2022006); National College Student Innovation and Entrepreneurship Training Program (grant number: 202110570033).

References

- 1 H. Sung, J. Ferlay, R. L. Siegel, M. Laversanne, I. Soerjomataram, A. Jemal and F. Bray, Global Cancer Statistics 2020: GLOBOCAN Estimates of Incidence and Mortality Worldwide for 36 Cancers in 185 Countries, *Ca-Cancer J. Clin.*, 2021, **71**, 209–249, DOI: [10.3322/caac.21660](#).
- 2 K. D. Miller, L. Nogueira, A. B. Mariotto, J. H. Rowland, K. R. Yabroff, C. M. Alfano, A. Jemal, J. L. Kramer and R. L. Siegel, Cancer treatment and survivorship statistics, 2019, *Ca-Cancer J. Clin.*, 2019, **69**, 363–385, DOI: [10.3322/caac.21565](#).
- 3 Y. Fukui, A. Saltiel and H. Hanafusa, Phosphatidylinositol-3 kinase is activated in v-src, v-yes, and v-fps transformed chicken embryo fibroblasts, *Oncogene*, 1991, **6**, 407–411, DOI: [10.1016/0027-5107\(91\)90045-P](#).
- 4 B. D. Manning and A. Toker, AKT/PKB signaling: navigating the network, *Cell*, 2017, **169**, 381–405, DOI: [10.1016/j.cell.2017.04.001](#).
- 5 M. Song, A. M. Bode, Z. Dong and M. Lee, AKT as a therapeutic target for cancer, *Cancer Res.*, 2019, **79**, 1019–1031, DOI: [10.1158/0008-5472.CAN-18-2738](#).
- 6 B. Bilanges, Y. Posor and B. Vanhaesebroeck, PI3K isoforms in cell signalling and vesicle trafficking, *Nat. Rev. Mol. Cell Biol.*, 2019, **20**, 515–534, DOI: [10.1038/s41580-019-0129-z](#).
- 7 H. Ellis and C. X. Ma, PI3K inhibitors in breast cancer therapy, *Curr. Oncol. Rep.*, 2019, **21**, 110, DOI: [10.1007/s11912-019-0846-7](#).
- 8 J. E. Burke and R. L. Williams, Synergy in activating class I PI3Ks, *Trends Biochem. Sci.*, 2015, **40**, 88–100, DOI: [10.1016/j.tibs.2014.12.003](#).
- 9 L. Zhang, Y. Li, Q. Wang, Z. Chen, X. Li, Z. Wu, C. Hu, D. Liao, W. Zhang and Z.-S. Chen, The PI3K subunits, P110 α and P110 β are potential targets for overcoming P-gp and BCRP-mediated MDR in cancer, *Mol. Cancer*, 2020, **19**, 10, DOI: [10.1186/s12943-019-1112-1](#).
- 10 D. A. Fruman, H. Chiu, B. D. Hopkins, S. Bagrodia, L. C. Cantley and R. T. Abraham, The PI3K pathway in human disease, *Cell*, 2017, **170**, 605–635, DOI: [10.1016/j.cell.2017.07.029](#).
- 11 J. Shi, D. Yao, W. Liu, N. Wang, H. Lv, G. Zhang, M. Ji, L. Xu, N. He, B. Shi and P. Hou, Highly frequent PIK3CA amplification is associated with poor prognosis in gastric cancer, *BMC Cancer*, 2012, **12**, 50–61, DOI: [10.1186/1471-2407-12-50](#).
- 12 M. A. Khan, V. K. Jain, M. Rizwanullah, J. Ahmad and K. Jain, PI3K/AKT/mTOR pathway inhibitors in triple-negative breast cancer: a review on drug discovery and future, *Drug Discovery Today*, 2019, **24**, 2181–2191, DOI: [10.1016/j.drudis.2019.09.001](#).
- 13 Y. R. Lee, M. Chen and P. P. Pandolfi, The functions and regulation of the PTEN tumour suppressor: new modes and prospects, *Nat. Rev. Mol. Cell Biol.*, 2018, **19**, 547–562, DOI: [10.1038/s41580-018-0015-0](#).
- 14 F. Martorana, G. Motta, G. Pavone, L. Motta, S. Stella, S. R. Vitale, L. Manzella and P. Vigneri, AKT inhibitors: new weapons in the fight against breast cancer?, *Front. Pharmacol.*, 2021, **12**, 662232, DOI: [10.3389/fphar.2021.662232](#).
- 15 Z. Xu, X. Han, D. Ou, T. Liu, Z. Li, G. Jiang, J. Liu and J. Zhang, Targeting PI3K/AKT/mTOR-mediated autophagy for tumor therapy, *Appl. Microbiol. Biotechnol.*, 2020, **104**, 575–587, DOI: [10.1007/s00253-019-10257-8](#).
- 16 H. L. Robbins and A. Hague, The PI3K/Akt pathway in tumors of endocrine tissues, *Front. Endocrinol.*, 2015, **6**, 188, DOI: [10.3389/fendo.2015.00188](#).
- 17 L. M. Thorpe, H. Yuzugullu and J. J. Zhao, PI3K in cancer: divergent roles of isoforms, modes of activation and therapeutic targeting, *Nat. Rev. Cancer*, 2015, **15**, 7–24, DOI: [10.1038/nrc3860](#).
- 18 B. Ramaswamy, Y. Lu, K. Y. Teng, G. Nuovo, X. Li, C. L. Shapiro and S. Majumder, Hedgehog signaling is a novel therapeutic target in tamoxifen-resistant breast cancer aberrantly activated by PI3K/AKT pathway, *Cancer Res.*, 2012, **72**, 5048–5059, DOI: [10.1158/0008-5472.can-12-1248](#).
- 19 S. Hong, H. Zhang, C. Xu and X. Zhao, Clinicopathological research and expression of PTEN/PI3K/Akt signaling pathway in non-small cell lung cancer, *Zhongguo Feiai Zazhi*, 2009, **12**, 889–892, DOI: [10.3779/j.issn.1009-3419.2009.08.11](#).
- 20 J. Zhu, T. Hou and X. Mao, Discovery of selective phosphatidylinositol 3-kinase inhibitors to treat hematological malignancies, *Drug Discovery Today*, 2015, **20**, 988–994, DOI: [10.1016/j.drudis.2015.03.009](#).
- 21 R. R. Yadav, S. K. Guru, P. Joshi, G. Mahajan, M. J. Mintoo, V. Kumar, S. S. Bharate, D. M. Mondhe, R. A. Vishwakarma, S. Bhushan and S. B. Bharate, 6-Aryl substituted 4-(4-cyanomethyl) phenylamino quinazolines as a new class of isoformselective PI3K-alpha inhibitors, *Eur. J. Med. Chem.*, 2016, **122**, 731–743, DOI: [10.1016/j.ejmech.2016.07.006](#).

- 22 W. Zhu, C. Chen, C. Sun, S. Xu, C. Wu, F. Lei, H. Xia, Q. Tu and P. Zheng, Design, synthesis and docking studies of novel thienopyrimidine derivatives bearing chromone moiety as mTOR/PI3K α inhibitors, *Eur. J. Med. Chem.*, 2015, **93**, 64–73, DOI: [10.1016/j.ejmech.2015.01.061](https://doi.org/10.1016/j.ejmech.2015.01.061).
- 23 T. Shao, J. Wang, J. G. Chen, X. M. Wang, H. Li, Y. P. Li, Y. Li, G. D. Yang, Q. B. Mei and S. Q. Zhang, Discovery of 2-methoxy-3-phenylsulfonamino-5-(quinazolin-6-yl or quinolin-6-yl)benzamides as novel PI3K inhibitors and anticancer agents by bioisostere, *Eur. J. Med. Chem.*, 2014, **75**, 96–105, DOI: [10.1016/j.ejmech.2014.01.053](https://doi.org/10.1016/j.ejmech.2014.01.053).
- 24 L. Zhu, Q. Luo, J. Bi, J. Ding, S. Ge and F. Chen, Galangin inhibits growth of human head and neck squamous carcinoma cells in vitro and in vivo, *Chem.-Biol. Interact.*, 2014, **224**, 149–156, DOI: [10.1016/j.cbi.2014.10.027](https://doi.org/10.1016/j.cbi.2014.10.027).
- 25 V. G. Abramson, A. B. Troxel, M. Feldman, C. Mies, Y. Wang, L. Sherman, S. McNally, A. Diehl and A. Demichele, Cyclin D1 b in human breast carcinoma and co expression with cyclin D1 a is associated with poor outcome, *Anticancer Res.*, 2010, **30**, 1279–1285.
- 26 J. Cao, H. Wang, F. Chen, J. Fang, A. Xu, W. Xi, S. Zhang, G. Wu and Z. Wang, Galangin inhibits cell invasion by suppressing the epithelial-mesenchymal transition and inducing apoptosis in renal cell carcinoma, *Mol. Med. Rep.*, 2016, **13**, 4238–4244, DOI: [10.3892/mmr.2016.5042](https://doi.org/10.3892/mmr.2016.5042).
- 27 W. He, H. Zhang and C. Yuan, Galangin enhanced antitumor effects of apatinib in gastric cancer SGC-7901 cells via PI3K/Akt and p38-MAPK signaling pathway, *Tianjin Yiyao*, 2019, **47**, 1020–1025, DOI: [10.11958/20190272](https://doi.org/10.11958/20190272).
- 28 E. H. Walker, M. E. Pacold, O. Perisic, L. Stephens, P. T. Hawkins, M. P. Wymann and R. L. Williams, Structural Determinants of Phosphoinositide 3-Kinase Inhibition by Wortmannin, LY294002, Quercetin, Myricetin and Staurosporine, *Mol. Cell*, 2000, **6**, 909–919, DOI: [10.1016/S1097-2765\(05\)00089-4](https://doi.org/10.1016/S1097-2765(05)00089-4).
- 29 T. Ikezoe, C. Nishioka, K. Bandobashi, Y. Yang, Y. Kuwayama, Y. Adachi, T. Takeuchi, H. P. Koeffler and H. Taguchi, Longitudinal inhibition of PI3K/Akt/mTOR signaling by LY294002 and rapamycin induces growth arrest of adult T-cell leukemia cells, *Leuk. Res.*, 2007, **31**, 673–682, DOI: [10.1016/j.leukres.2006.08.001](https://doi.org/10.1016/j.leukres.2006.08.001).
- 30 M. E. Abdallah, M. Z. El-Readi, M. A. Althubiti, R. A. Almairani, A. M. Ismail, S. Idris, B. Refaat, W. H. Almalki, A. T. Babakr, M. H. Mukhtar, A. N. Abdalla and O. F. Idris, Tamoxifen and the PI3K Inhibitor: LY294002 Synergistically Induce Apoptosis and Cell Cycle Arrest in Breast Cancer MCF-7 Cells, *Molecules*, 2020, **25**, 3355, DOI: [10.3390/molecules25153355](https://doi.org/10.3390/molecules25153355).
- 31 Z. Zheng, J. A. Pinson, S. J. Mountford, S. Orive, S. M. Schoenwaelder, D. Shackelford, A. Powell, E. M. Nelson, J. R. Hamilton, S. P. Jackson, I. G. Jennings and P. E. Thompson, Discovery and antiplatelet activity of a selective PI3K beta inhibitor (MIPS-9922), *Eur. J. Med. Chem.*, 2016, **122**, 339–351, DOI: [10.1016/j.ejmech.2016.06.010](https://doi.org/10.1016/j.ejmech.2016.06.010).
- 32 T. P. Heffron, B. Wei, A. Olivero, S. T. Staben, V. Tsui, S. Do, J. Dotson, A. J. Folkes, P. Goldsmith, R. Goldsmith, J. Gunzner, J. Lesnick, C. Lewis, S. Mathieu, J. Nonomiya, S. Shuttleworth, D. P. Sutherland, N. C. Wan, S. Wang, C. Wiesmann and B. Y. Zhu, Rational design of phosphoinositide 3-kinase alpha inhibitors that exhibit selectivity over the phosphoinositide 3-kinase beta isoform, *J. Med. Chem.*, 2011, **54**, 7815–7833, DOI: [10.1021/jm2007084](https://doi.org/10.1021/jm2007084).
- 33 C. Chaussade, G. W. Rewcastle, J. D. Kendall, W. A. Denny, K. Cho, L. M. Grønning, M. L. Chong, S. H. Anagnostou, S. P. Jackson, N. Daniele and P. R. Shepherd, Evidence for functional redundancy of class IA PI3K isoforms in insulin signalling, *Biochem. J.*, 2007, **404**, 449–458, DOI: [10.1042/BJ20070003](https://doi.org/10.1042/BJ20070003).
- 34 M. Abazeed, D. Adams, K. Hurov, P. Tamayo, C. Creighton, D. Sonkin, A. Giacomelli, S. Schreiber, P. Hammerman and M. Meyerson, Integrative radiogenomic profiling of squamous cell lung cancer, *Cancer Res.*, 2013, **73**, 6289–6298, DOI: [10.1016/j.jrobp.2013.06.356](https://doi.org/10.1016/j.jrobp.2013.06.356).
- 35 C. Massacesi, E. Di Tomaso, P. Urban, C. Germa, C. Quadt, L. Trandafir, P. Aimone, N. Fretault, B. Dharan, R. Tavorath and S. Hirawat, PI3K inhibitors as new cancer therapeutics: implications for clinical trial design, *Oncotargets Ther.*, 2016, **9**, 203–210, DOI: [10.2147/OTT.S89967](https://doi.org/10.2147/OTT.S89967).
- 36 G. Luo, Y. Ma, X. Liang, G. Xie, Y. Luo, D. Zha, S. Wang, L. Yu, X. Zheng, W. Wu and C. Zhang, Design, synthesis and antitumor evaluation of novel 5-methylpyrazolo[1,5-a]pyrimidine derivatives as potential c-Met inhibitors, *Bioorg. Chem.*, 2020, **104**, 104356, DOI: [10.1016/j.bioorg.2020.104356](https://doi.org/10.1016/j.bioorg.2020.104356).
- 37 Y. Luo, W. Wu, D. Zha, W. Zhou, C. Wang, J. Huang, S. Chen, L. Yu, Y. Li, Q. Huang, J. Zhang and C. Zhang, Synthesis and biological evaluation of novel ligustrazine-chalcone derivatives as potential anti-triple negative breast cancer agents, *Bioorg. Med. Chem. Lett.*, 2021, **47**, 128230, DOI: [10.1016/j.bmcl.2021.128230](https://doi.org/10.1016/j.bmcl.2021.128230).
- 38 M. Manikanta, S. Vikas, C. Pramila and V. Suvarna, A critical review on anticancer mechanisms of natural flavonoid puerarin, *Anti-Cancer Agents Med. Chem.*, 2020, **20**, 678–686, DOI: [10.2174/1871520620666200227091811](https://doi.org/10.2174/1871520620666200227091811).
- 39 D. Y. Li, G. Du, X. P. Gong, J. Guo, J. Zhang, C. Chen, Y. Xue, H. Zhu and Y. Zhang, Hyperattennins L and M, two new polyprenylated acylphloro-gluconols with adamantyl and homoadamantyl core structures from *Hypericum attenuatum*, *Fitoterapia*, 2018, **125**, 130–134, DOI: [10.1016/j.fitote.2017.12.020](https://doi.org/10.1016/j.fitote.2017.12.020).